Gynecologic Oncology 132 (2014) 715–721

Contents lists available at ScienceDirect

Gynecologic Oncology

journal homepage: www.elsevier.com/locate/ygyno

Identification of endometrioid endometrial carcinoma-associated microRNAs in tissue and plasma

Ozora Tsukamoto [a], Kiyonori Miura [a,*], Hiroyuki Mishima [b], Shuhei Abe [a], Masanori Kaneuchi [a], Ai Higashijima [a], Shoko Miura [a], Akira Kinoshita [b], Koh-ichiro Yoshiura [b], Hideaki Masuzaki [a]

[a] Department of Obstetrics and Gynecology, Nagasaki University Graduate School of Biomedical Sciences, Nagasaki, Japan
[b] Department of Human Genetics, Nagasaki University Graduate School of Biomedical Sciences, Nagasaki, Japan

HIGHLIGHTS

- A set of endometrioid endometrial carcinoma (EEC)-associated miRNAs in tissue and plasma was identified by next-generation sequencing approach.
- EEC-associated miRNAs in tissues and plasma samples could distinguish EEC sample from NE sample with high accuracy.
- EEC-associated miRNA levels in EEC tissues and plasma samples were associated with pathological characteristics.

ARTICLE INFO

Article history:
Received 4 November 2013
Accepted 16 January 2014
Available online 31 January 2014

Keywords:
Endometrioid endometrial carcinoma
Next-generation sequencing
MiRNA
Tissue
Plasma

ABSTRACT

Objective. This study aimed to identify a set of endometrioid endometrial carcinoma EEC-associated microRNAs (miRNAs) in tissue and plasma, and evaluate their clinical significance.

Methods. A set of EEC-associated miRNAs in tissue and plasma was identified by next-generation sequencing (NGS), which could enable in-depth characterization of the global repertoire of miRNAs.

Results. NGS identified 11 candidate EEC-associated miRNAs. Quantitative reverse-transcriptase PCR identified 8 EEC-associated miRNAs in tissue (upregulated: miR-499, miR-135b, miR-205, downregulated: miR-10b, miR-195, miR-30a-5p, miR-30a-3p and miR-21). Expression of hsa-miR-499 in International Federation of Gynecology and Obstetrics (FIGO) Stage IA and Grade 1 tissues was significantly lower than in others (FIGO Stage IB or more advanced, and Grade 2 or 3). By receiver operating characteristic (ROC) curve analysis, compared with single EEC-associated miRNA, two miRNA signatures (miR135b/miR195 and miR135b/miR30a-3p) could distinguish between EEC and normal endometrial tissue samples yielding a high area under the curve (AUC) of 0.9835 [95% confidence interval (CI): 0.9677–1.0], and 0.9898 (95% CI: 0.9677–1.0), respectively. As possible non-invasive markers for EEC, four EEC-associated miRNAs (increased level: miR-135b and miR-205, decreased-level: miR-30a-3p and miR-21) in plasma were identified. Circulating levels of three EEC-associated miRNAs (miR-135b, miR-205 and miR-30a-3p) in plasma were significantly decreased after hysterectomy. ROC curves analysis revealed that miR-135b and miR-205 levels in plasma yielded AUCs of 0.9722 (95% CI: 0.913–1.0) and 1.0 (95% CI: 1.0–1.0), respectively.

Conclusion. Measurement of tissue and plasma EEC-associated miRNAs may be useful for early detection, diagnostic, and follow-up tests for EEC.

Introduction

Endometrial cancer is a common malignancy of the female reproductive tract. The most dominant subtype, endometrioid endometrial carcinoma (EEC) accounts for ~80% of cases [1]. Accumulation of several genetic and epigenetic alternations in oncogenes and tumor suppressor genes is involved in the development of endometrial carcinoma [2]. However, such alterations are not uniformly found in all EEC cases, and information regarding the molecular mechanisms of EEC etiology is still limited. The search for novel molecular markers for early detection and predicting outcomes has been ongoing in most cancers with a view to identifying molecular targets for therapeutic agents.

MicroRNAs (miRNAs) are non-protein-coding small RNAs (21–25 nucleotides) that function as regulators of gene expression by antisense complimentarily to specific mRNAs [3,4]. As miRNAs are expressed in tissue-specific patterns [3], miRNAs predominantly expressed in EEC tissues are probably involved in cell proliferation, differentiation, apoptosis, and carcinogenesis of the endometrium [5,6]. Recently, by searching a panel of microarray assays, miRNA signatures in tissue and

* Corresponding author at: Department of Obstetrics and Gynecology, Nagasaki University Graduate School of Biomedical Sciences, 1-7-1 Sakamoto, Nagasaki 852-8501, Japan. Fax: +81 95 819 7365.
E-mail address: kiyonori@nagasaki-u.ac.jp (K. Miura).

0090-8258/$ – see front matter
http://dx.doi.org/10.1016/j.ygyno.2014.01.029

plasma could be used to distinguish EEC from normal endometrium (NE) [7,8]. This suggests that EEC-associated miRNAs have the potential to be developed as novel diagnostic and therapeutic molecules. However, the data regarding EEC-associated miRNAs in tissue and plasma are limited; therefore, investigation of EEC-associated miRNAs is likely to shed light on the molecular mechanisms of EEC etiology.

Microarray technology is high throughput, but can only detect a limited number of miRNAs because of the nature of probe hybridization [9]. Next-generation sequencing (NGS) technology using Illumina technology generates short reads (35 bp) but more than 1 million bp of sequence data per run, and can be used to measure the abundance of small-RNA sequences in a sample. miRNAs are only 21–25 bp in length; therefore, this technology can enable in-depth characterization of the global repertoire of miRNAs [10].

In this study, to get a clue regarding novel diagnostic and therapeutic molecules of EEC, we tried to identify EEC-associated miRNAs in tissue and plasma. First, by comparative analysis of NGS-generated miRNA expression profiles of EEC tissue, NE tissue and blood cells from the same patient, we selected candidate EEC-associated miRNAs, whose expression level was negative in the blood of patients, and in EEC tissues was >2 times up- or downregulated compared with that in NE tissue. Second, by comparative analysis of EEC and NE tissues using real-time quantitative RT-PCR (qRT-PCR), we identified EEC-associated miRNAs in tissue. Subsequently, to identify and characterize EEC-associated miRNAs in plasma, the circulating levels of EEC-associated miRNA in plasma in women with EEC or NE. Finally, the relationship between EEC-associated miRNA expression and clinicopathological characteristics, and the diagnostic value of EEC-associated miRNA expression in tissue and plasma were analyzed tentatively.

Materials and methods

Sample collection

Study subjects were recruited at the Department of Obstetrics and Gynecology, Nagasaki University Hospital, Japan. All samples were obtained after receiving written informed consent, and the study protocol was approved by the Institutional Review Board for Ethical, Legal and Social Issues of Nagasaki University.

For NGS analysis, EEC tissue, NE tissue, and blood cells were obtained from an identical patient with International Federation of Obstetricians and Gynecologists (FIGO) Stage IA (Grade 1) EEC. EEC and NE tissue samples were obtained immediately after total hysterectomy with bilateral salpingo-oophorectomy. EEC was diagnosed by endometrial biopsy prior to the operation. Diagnosis of EEC and NE tissue was confirmed by pathological analysis. EEC and NE tissue samples were placed in RNAlater (Ambion, Austin, TX, USA). The blood samples (7 mL) were collected before the operation and placed in tubes containing EDTA. Using a mirVana miRNA Isolation Kit (Ambion), total RNA containing small RNA molecules was extracted from each sample immediately after sampling. Quality assessment and concentration measurements of total RNA, including small RNAs, were performed using a Bioanalyzer (Agilent Technologies, South Queensferry, UK) and a NanoDrop spectrophotometer (Thermo Fisher Scientific, Waltham, MA, USA), respectively.

For subsequent expression analysis by qRT-PCR, EEC tissues were obtained from 28 cases of EEC (EEC group) and NE tissues from 14 cases of non-EEC (NE group). In addition to total hysterectomy with bilateral salpingo-oophorectomy, lymphadenectomy was performed in 25 cases. Tumor stage was determined according to 2009 revised FIGO classification [11]. In cases of NE, total hysterectomy was performed because of uterine myoma. Final diagnosis of EEC or NE was confirmed by pathological analysis. None of the EEC patients had a history of other malignant disease or had received neoadjuvant therapy. After the operation, patients were submitted to radiotherapy and/or chemotherapy according to FIGO guidelines. Between the EEC and NE groups, there were no significant differences in body mass index (BMI), history of parity, smoking, diabetes, or family history of endometrial cancer (data not shown). The mean (SD) patient age was 60.6 (10.8) years in the EEC group and 42.8 (5.1) years in the NE group (Student's t test, $P < 0.001$). Clinicopathological characteristics in the EEC group are listed in Supplementary Table 1.

To obtain cell-free plasma miRNAs, blood samples (7 mL) were collected from 12 cases of EEC and 12 of NE. Blood sampling was performed 1 day before the operation and 7 days after. Between the EEC and NE groups, there were no significant differences in BMI, history of parity, smoking, diabetes, or family history of endometrial cancer (data not shown). The mean (SD) patient age was 50.8 (8.3) years in the EEC group and 36.5 (8.3) years in the NE group (Student's t test, $P = 0.001$). Pathological characteristics in the EEC group are listed in Supplementary Table 2. Cell-free plasma samples were prepared from the blood by a double centrifugation method as described previously [12]. Total RNA containing small RNA molecules was extracted from 1.2 mL cell-free plasma samples as described previously [12]. Extracted total RNAs were stored at −80 °C. Although there were differences in age between the EEC and NE groups in both tissue and plasma, there was no significant correlation between expression of studied miRNAs and age of patients (data not shown).

In miRNA expression analysis in endometrial tissue, there is no consensus on universal endogenous normalization controls because small RNAs, including RNU48 and RNU6B, have been suggested as reference RNAs, but exhibit high variability [13]. In addition, it is recommended that the quantitative mRNA measurements in plasma are expressed as an absolute concentration [14]. Therefore, we considered that the quantitative miRNA measurements may be the same as quantitative mRNA measurements in plasma. In this study, absolute real-time qRT-PCR analysis was performed.

Small RNA library construction and NGS analysis

To screen for EEC-associated miRNAs, NGS was applied to a set of EEC tissues, NE tissues and blood from the same EEC patient. Isolation of total RNA including small RNAs, their quality assessment, concentration measurements, small RNA library construction, NGS and miRNA mapping were performed as described previously [15–18].

To compare miRNA levels across data sets, the sequencing read count for each miRNA was normalized to the total read count of 1,000,000 in each sample, and expressed as reads per million (RPM) [15–17]. For mapped data, when the normalized miRNA read count was negative in patient's blood, and was >2 times up- or downregulated in EEC tissues than in NE tissue, these miRNAs were selected as candidate EEC-associated miRNAs. These miRNAs were then analyzed by RT-PCR in tissue and plasma from the EEC and NE group.

Real-time qRT-PCR analysis of miRNAs

All specific primers and TaqMan probes were purchased from TaqMan MicroRNA Assays (Applied Biosystems). Real-time qRT-PCR of miRNAs in tissues and plasma samples was performed as described previously [12,15]. For each miRNA assay, we prepared a calibration curve by 10-fold serial dilution of single-stranded cDNA oligonucleotides corresponding to each miRNA sequence from 1.0×10^2 to 1.0×10^8 copies/mL. Each sample and each calibration dilution were analyzed in triplicate. Each assay could detect down to 100 RNA copies/mL. Every batch of amplifications included three water blanks as negative controls for each of the reverse transcription and PCR steps. All data were collected and analyzed using an ABI Prism 7900 Sequence Detector (Applied Biosystems).

Statistical analysis

Patient backgrounds were compared by Student's t test and Pearson's χ^2 test for continuous and discrete variables, respectively, of

EEC and NE cases. Absolute quantification data were analyzed with SDS 2.3 software (Applied Biosystems). The expression levels of EEC-associated miRNAs in tissues and the cell-free plasma concentrations of EEC-associated miRNAs in cases of EEC and NE were converted into multiples of the median (MoM) of concentration in the cases of NE. Differences between the two groups were evaluated with Mann–Whitney's *U* test or Kruskal–Wallis test. Changes in the cell-free plasma concentration of EEC-associated miRNAs before and after the operation were compared by the Wilcoxon signed-rank test. Statistical analyses were performed with SPSS version 19 (IBM Japan, Tokyo, Japan). To determine the ability of miRNAs to classify EEC and NE samples, receiver operating characteristic (ROC) curves were plotted with an R package, pROC [19]. To develop miRNA signatures featuring the best accuracy in distinguishing between EEC and NE samples a multivariate logistic regression model was utilized. Evaluation of obtained regression models was performed with the Wald test. Statistical analyses were performed using R (R Core Team, Vienna, Austria). Significant differences were defined as $P < 0.05$.

Results

Screening of candidate EEC-associated miRNAs by NGS

NGS analysis yielded 20,674,015 reads from EEC tissue, 19,107,722 reads from blood cells, and 20,375,081 reads from NE tissue. All the above sequence data were deposited in DDBJ Sequence Read Archive (DRA) (accession ID: DRA001166). High-throughput sequencing assays can be susceptible to noise and variability; therefore, measurement of miRNA expression was normalized using the library size (1,000,000 reads). Eleven candidate EEC-associated miRNAs were identified (Table 1). Candidate EEC-associated miRNAs identified were located on various chromosomal regions. Out of 11 candidate EEC-associated miRNAs, 5 (miR-10b, miR-499, miR-184, miR-195 and miR-135b) were upregulated in EEC tissue, while 6 (miR-203, miR-10a, miR-30a-5p, miR-205, miR-30a-3p and miR-21) were downregulated in EEC tissue than NE (Table 1).

Confirmation of EEC-associated miRNAs in tissue by qRT-PCR

Expression levels of the 11 candidate EEC-associated miRNAs in 28 EEC and 14 NE tissues were measured by qRT-PCR. Eight miRNAs showed significantly different expression between EEC and NE tissues, and were identified as EEC-associated miRNAs in tissue. The expression levels of 3 EEC-associated miRNAs (miR-499, miR-135b and miR-205) were significantly higher in EEC than NE tissues (Mann–Whitney *U* test, $P = 0.003$, $P < 0.001$ and $P = 0.002$, respectively), while those of 5 EEC-associated miRNAs (miR-10b, miR-195, miR-30a-5p, miR-30a-3p and miR-21) were significantly downregulated in EEC tissue (Mann–Whitney *U* test, $P = 0.006$, $P < 0.001$, $P = 0.019$, $P = 0.001$, and $P = 0.011$, respectively; Table 2). Meanwhile, there was no significant difference in the levels of 3 candidate EEC-associated miRNAs (miR-184, miR-203 and miR-10a) between EEC and NE tissues (Table 2). Using a database search of predicted miRNA targets in mammals (www.targetscan.org), we searched the candidate target mRNAs of EEC-associated miRNAs in tissue. Three mRNAs (MutS homolog 2: MSH2, Leukotriene B4 12-hydroxydehydrogenase: LTB4DH and IκB kinase α: IKKα) were selected as common target mRNAs of 3 upregulated EEC-associated miRNAs in EEC tissue, while there was no common target mRNAs of 5 downregulated EEC-associated miRNAs.

Identification of EEC-associated miRNAs in plasma

Regarding the 8 EEC-associated miRNAs in tissue, circulating levels of each miRNA in plasma from 12 women with EEC and 12 with NE tissue were measured by qRT-PCR. Four miRNAs showed significantly different circulating levels between the EEC and NE groups, and were identified as EEC-associated miRNAs in plasma. The expression levels of 2 EEC-associated miRNAs (miR-135b and miR-205) were significantly higher in plasma samples from the EEC group than the NE group (Mann–Whitney *U* test, $P < 0.001$), while those of 2 EEC-associated miRNAs (miR-30a-3p and miR-21) were significantly lower in plasma samples from the EEC group than the NE group (Mann–Whitney *U* test, $P = 0.009$ and $P = 0.033$, respectively). Meanwhile, there was no significant difference in the levels of 4 EEC-associated miRNAs (miR-10b, miR-30a-5p, miR-195 and miR-499) between plasma samples from the EEC and NE groups (Table 3).

Identification of EEC-associated miRNAs that showed significantly decreased concentrations in plasma after hysterectomy

The 4 EEC-associated miRNAs that showed significantly increased or decreased levels in plasma in the EEC group compared with the NE group (Table 3, increased level: miR-135b and miR-205, decreased level: miR-30a-3p and miR-21) were selected for analysis before and after hysterectomy. The plasma concentrations of 3 miRNAs (Table 4, miR-135b, miR-205 and miR-30a-3p) were significantly decreased after hysterectomy (Wilcoxon signed-rank tests, $P = 0.003$, Table 3), and were considered as possible molecular markers in plasma. Meanwhile, there was no significant difference in the plasma level of hsa-miR-21 before and after hysterectomy (Table 3).

Relationship between EEC-associated miRNA expression and clinicopathological characteristics

To investigate the clinical significance of EEC-associated miRNAs in tissue and plasma, we compared EEC-associated miRNA expression in groups distinguished based on FIGO stage, histopathological grade, or relapse. Significant relationships were found between expression of miR-499 and FIGO stage, and between expression of miR-205 and histological grade. The expression level of miR-499 in 14 cases of FIGO Stage

Table 1
Candidate EEC-associated miRNAs detected by next-generation sequencing analysis.

miRNA	Chromosome localization	Blood cell (reads per million)	EEC tissue (reads per million)	NE tissue (reads per million)	EEC/NE
hsa-miR-10b	2q31.1	3	2220	770	2.88
hsa-miR-499	20q11.22	0	2010	705	2.85
hsa-miR-184	15q25.1	11	2006	851	2.36
hsa-miR-195	17p13.1	0	12,901	6320	2.04
hsa-miR-135b	1q32.1	0	133	66	2.02
hsa-miR-203	14q32.33	0	1712	3514	0.48
hsa-miR-10b	17q21.32	2	263	602	0.44
hsa-miR-30a-5p	6q13	50	15,732	45,694	0.34
hsa-miR-205	1q32.2	0	285	1356	0.21
hsa-miR-30a-3p	6q13	29	1610	9476	0.17
hsa-miR-21	17q23.1	30	219	1369	0.16

Normalized read counts are described as reads per million.

Table 2
Expression of candidate EEC-associated miRNAs in carcinoma tissues from patients with EEC group and NE tissues from patients without carcinoma.

miRNA	NE group ($n = 14$)	EEC group ($n = 28$)	P value
miR-10b	1.0 (0.68–1.62)	0.79 (0.17–2.81)	0.006
miR-499	1.0 (0.28–1.99)	2.49 (0.22–40.08)	0.003
miR-184	1.0 (0.1–18.2)	0.82 (0.06–169.3)	NS
miR-195	1.0 (0.024–1.96)	0.32 (0.10–0.87)	<0.001
miR-135b	1.0 (0.57–3.40)	5.13 (0.49–15.13)	<0.001
miR-203	1.0 (0.38–1.49)	1.13 (0.18–3.92)	NS
miR-10b	1.0 (0.29–1.55)	0.79 (0.17–2.81)	NS
miR-30a-5p	1.0 (0.23–2.0)	0.61 (0.27–1.62)	0.019
miR-205	1.0 (0.06–4.07)	2.47 (0.0–6.19)	0.002
miR-30a-3p	1.0 (0.54–2.04)	0.53 (0.1–2.45)	0.001
miR-21	1.0 (0.39–2.76)	0.64 (0.27–1.22)	0.011

Expression levels are described as MoM values [median (minimum – maximum)]. Significant differences between groups were analyzed by Mann–Whitney U test. $P < 0.05$ was considered significant.
NS, not significant.

II or more advanced was significantly higher than that in 4 cases of FIGO Stage IA and IB (Mann–Whitney U test, $P = 0.019$, Supplementary Table 1). The expression level of miR-205 in EEC cases with Grade 3 tumor ($n = 2$) was significantly higher than that in cases with Grade 1 ($n = 15$) and 2 ($n = 11$) tumors (Kruskal–Wallis test, $P = 0.024$, Supplementary Table 1). The expression level of miR-499 in 7 cases of FIGO Stage IA and Grade 1 tumor was significantly lower than in 21 cases of other tumors (FIGO Stage IB or more advanced, and Grade 2 or 3) (Mann–Whitney U test, $P = 0.047$, Table 4). Meanwhile, there was no significant difference in the tissue levels of all EEC-associated miRNAs between groups distinguished according to the presence of lymph node metastasis or occurrence of relapse (Table 4).

Circulating miRNA levels of EEC-associated miRNAs in plasma were compared in groups distinguished according to FIGO stage and histopathological grade. We compared FIGO Stage IA Grade 1 tumors with others (more advanced FIGO stage and/or histopathological grade). The plasma concentration of miR-21 in 4 cases of FIGO Stage IA and Grade 1 tumors was significantly higher than that in 8 cases of more advanced tumors (Mann–Whitney U test, $P = 0.017$, Table 5). Meanwhile, there was no significant difference in the plasma concentrations of other EEC-associated miRNAs (miR-135b, miR-205 and miR-30a-3p) and carbohydrate antigen (CA)125 before and after hysterectomy (Table 5).

Diagnostic value of EEC-associated miRNA expression in tissue and plasma

ROC curves for discriminating EEC samples from NE were constructed based on EEC-associated miRNA expression in tissues (EEC, $n = 28$; NE, $n = 14$). Analysis of the ROCs revealed high area under curve (AUC) values for each EEC-associated miRNA in tissues (Fig. 1): miR-499, miR-30a-5p, miR-21, miR-10b, miR-205, miR-30a-3p, miR-195 and miR-135b yielded AUC of 0.7143 [95% confidence interval (CI): 0.5537–0.8749], 0.7245 (95% CI: 0.5445–0.9045), 0.7423 (95% CI: 0.5744–0.9103), 0.7602 (95% CI: 0.6132–0.9072), 0.8112 (95% CI: 0.666–0.9565), 0.8265 (95% CI: 0.6953–0.9578), 0.8736 (95% CI: 0.7145–1.0) and 0.9184 (95% CI: 0.8285–1.0), respectively (Fig. 1A). The miRNA signatures consisting of 2 miRNAs yielded elevated AUCs in comparison to single miRNAs. miR135b/miR195 and miR135b/miR30a-3p yielded AUCs of 0.9835 (95% CI: 0.9677–1.0, $P < 0.048$, Wald test, Fig. 1A), and 0.9898 (95% CI: 0.9677–1.0, $P < 0.038$, Wald test, Fig. 1A), respectively.

ROC curves for discriminating women with EEC from those with NE were constructed based on EEC-associated miRNA levels in plasma samples (EEC, $n = 12$; NE, $n = 12$). Analysis of the ROCs revealed high AUC values for each EEC-associated miRNA in plasma (Fig. 1B); miR-21, miR-30a-3p, miR-135b and miR-205 yielded AUC of 0.7569 (95% CI: 0.5611–0.9528), 0.8125 (95% CI: 0.6381–0.9869), 0.9722 (95% CI: 0.913–1.0) and 1.0 (95% CI: 1.0–1.0), respectively.

Discussion

In this study, we identified EEC-associated miRNAs in tissue and plasma, and evaluated their clinical significance.

NGS can be used to investigate all known and unknown miRNAs, while oligonucleotide microarray methods can only be used to examine a limited number of known miRNAs present on each array. Therefore, using NGS allows whole genome analysis to be performed to identify candidate miRNAs that are differentially expressed. In addition, the miRNA expression in each case of EEC depends on the heterogeneity of cancer. Our NGS analyses identified 11 candidate EEC-associated miRNAs (upregulated: miR-10b, miR-499, miR-184, miR-19 and miR-135b, downregulated: miR-203, miR-10a, miR-30a-5p, miR-205, miR-30a-3p and miR-21) at various chromosomal regions. Although all miRNAs were previously known, nine of the 11 were newly identified as candidate EEC-associated miRNAs (except for miR-203 and miR-205) that had not been identified in previous microarray studies [5–7,20]. Therefore, this indicates that NGS enables a more in-depth

Table 3
Circulating levels of EEC-associated miRNAs in plasma samples from patients without carcinoma (NE plasma) and patients with EEC (EEC plasma) before and after surgery.

miRNA	A	B	C	P value	
	NE plasma ($n = 12$)	EEC plasma before operation ($n = 12$)	EEC plasma after operation ($n = 11$)	A vs B	B vs C
miR-135b	1.0 (0.57–3.40)	5.13 (0.49–15.13)	0.0062 (0–0.96)	<0.001	0.003
miR-205	1.0 (0.06–4.07)	2.34 (0.0–6.19)	0.56 (0.34–0.94)	<0.001	0.003
miR-30a-3p	1.0 (0.54–2.04)	0.53 (0.096–2.25)	0.062 (0–0.12)	0.009	0.003
miR-21	1.0 (0.39–2.76)	0.64 (0.27–1.22)	0.59 (0.023–3.11)	0.033	NS
miR-10b	1.0 (0.34–2.49)	0.745 (0.05–1.55)	–	NS	–
miR-30a-5p	1.0 (0.21–2.74)	0.48 (0.05–1.3)	–	NS	–
miR-195	1.0 (0.24–2.1)	0.615 (0.05–1.73)	–	NS	–
miR-499	ND	ND	–	–	–

Expression levels are described as MoM values [median (minimum – maximum)]. Significant differences between control and EEC plasma before surgery were analyzed by Mann–Whitney U test, and significant differences between EEC plasma before and after operation were analyzed by Wilcoxon singed-rank test. $P < 0.05$ was considered significant.
–, not analyzed; ND, not detected; NS, not significant.

Table 4
Association between clinicopathological characteristics and EEC-associated miRNA levels in EEC tissues.

	FIGO stage and grade			Lymph node metastasis			Relapse		
	IA G1 ($n = 7$)	Others[a] ($n = 21$)	*P* value	− ($n = 21$)	+ ($n = 4$)	*P* value	− ($n = 25$)	+ ($n = 3$)	*P* value
miR-135b	5.64 (3.51–12.13)	4.39 (0.49–15.13)	NS	5.55 (0.49–12.13)	6.03 (1.49–15.13)	NS	5.67 (0.86–15.13)	4.09 (0.49–4.68)	NS
miR-205	2.92 (1.14–6.09)	2.24 (0–6.19)	NS	2.14 (0–6.19)	3.03 (1.43–6.12)	NS	2.74 (0–6.19)	1.43 (1.4–2.34)	NS
miR-21	0.89 (0.43–1.22)	0.58 (0.27–0.96)	NS	0.7 (0.32–1.22)	0.55 (0.46–0.96)	NS	0.7 (0.27–1.22)	0.55 (0.32–0.81)	NS
miR-30a-3p	0.595 (0.22–2.45)	0.43 (0.1–2.15)	NS	0.28 (0.24–0.45)	0.57 (0.13–2.45)	NS	0.55 (0.1–2.45)	0.45 (0.2–0.72)	NS
miR-499	1.09 (0.41–2.54)	2.92 (0.22–40.08)	0.047	2.09 (0.22–40.48)	5.24 (2.48–26.26)	NS	2.48 (0.21–40.48)	3 (2.73–7.21)	NS
miR-10b	0.8 (0.49–2.59)	0.66 (0.17–2.81)	NS	0.79 (0.21–2.81)	0.88 (0.3–1.15)	NS	0.79 (0.17–2.81)	0.85 (0.56–1.15)	NS
miR-30a-5p	0.69 (0.39–1.26)	0.61 (0.27–1.62)	NS	0.62 (0.27–1.62)	0.58 (0.46–0.68)	NS	0.61 (0.28–1.62)	0.61 (0.27–1.39)	NS
miR-195	0.28 (0.13–0.87)	0.35 (0.1–0.74)	NS	0.26 (0.13–0.87)	0.35 (0.1–0.54)	NS	0.33 (0.13–0.87)	0.18 (0.1–0.74)	NS

Expression levels of miRNAs are described as MoM values [median (minimum — maximum)]. Significant differences between groups were analyzed by Mann–Whitney *U* test. $P < 0.05$ was considered significant.
NS, not significant.
[a] Includes tumors with more advanced FIGO stage and/or histopathological grade than Stage IA, Grade 1.

characterization of the global repertoire of miRNAs compared with oligonucleotide microarray analysis and/or the heterogeneity of cancer because the discovery set used for NGS analysis was obtained from a single cancer patient, a limitation of this study. Therefore, it is critical to explore additional studies of miRNAs based on the heterogeneity of EEC. Consistent with a previous study, several dysregulated miRNAs in EEC tissues were identified in our analyses [5–7,20]. However, in previous studies of EEC tissues, miR-200 family, miR-9, miR-203, miR-205 and miR-210 were upregulated, while miR-410, miR-17-5p, miR-214, miR-99a,b, miR-199b, miR-100, miR-20a, miR-221, miR-222 and miR-424 were downregulated [5,7,20–26]. The discrepancy between our study and the previous studies reflects the difference in the way to select the candidate EEC-associated miRNAs at the beginning of each study. Previous studies have selected EEC-associated miRNAs with predominantly dysregulated expression in the EEC tissues at the beginning of their study [7]. In contrast, we selected the miRNAs that had predominantly dysregulated expression in EEC tissues compared with NE tissues, but negative expression (<100 read counts) in blood cells as candidate EEC-associated miRNAs. This was because one of our goals was to identify the EEC-associated miRNAs in plasma as non-invasive diagnostic markers for EEC. Another reason for the discrepancy between the present and previous studies may be related to the method of obtaining samples for high-throughput analysis. Previous studies obtained EEC and NE samples from different individuals. However, each case had a heterogeneous background and each miRNA expression pattern in EEC and NE was affected by various factors, for example, the phase during the menstrual cycle, and the background affecting the molecular pathways of EEC and NE differed among individuals. Therefore, in the present study, to make uniform the influence of backgrounds affecting miRNA expression in EEC and NE, we compared EEC and NE tissue from the same EEC patient (FIGO Stage IA, Grade 1) at the same time.

Subsequent confirmation analysis using qRT-PCR identified 8 EEC-associated miRNAs in tissue (upregulated: miR-499, miR-135b and miR-205, downregulated: miR-10b, miR-195, miR-30a-5p, miR-30a-3p and miR-21). miR-205 was upregulated in the qRT-PCR study, although it was downregulated in the NGS experiment. Additionally, miR-10b and miR-195 were downregulated in the qRT-PCR study, although they were upregulated in the NGS experiment. This discrepancy was also found in a previous study [7], and might have been because single cases were analyzed by NGS but multiple cases by qRT-PCR.

We identified novel and already known EEC-associated miRNAs [5,7,20–26]. miR-205 is frequently dysregulated in many human cancers, suggesting its important roles in initiation and progression of cancer. Previous studies identified significantly overexpressed hsa-miR-205 in endometrial cancer compared with NE tissue, and JPH4, ESRRG and PTEN were the candidate tumor suppressor genes in EEC [5,27,28]. In contrast, miRNA-205 was significantly suppressed in renal cancer cell lines and tumors when compared with normal tissues and a non-malignant cell line [29]. The expression of miRNA-205 is significantly high in some malignancies but significantly low in other malignancies, depending on the organs from which the malignancy comes. These observations suggest that a miRNA has more than one target mRNA.

By using the database search, 3 mRNAs (MSH2, LTB4DH and IKKα) were selected as common targets of 3 up-regulated EEC-associated miRNAs in EEC tissue. An oncogenic miRNA acts as an oncogene and has increased expression in tumor cells, while a tumor suppressor miRNA acts as a tumor suppressor gene and has decreased expression in tumor cells. All 3 candidate target mRNAs are tumor suppressor genes [30–34], thus, it is compatible that they are candidate target mRNAs of upregulated EEC-associated miRNAs (oncogenic miRNAs) in EEC tissue.

The relationship between EEC-associated miRNA expression in EEC tissue and clinicopathological characteristics was investigated. The expression level of has-miR-499 in tissues of FIGO Stage II or more

Table 5
Association between pathological characteristics, EEC-associated miRNA levels and CA 125 levels in plasma from patients with EEC.

	FIGO stage and grade		
	IA G1 ($n = 4$)	Others[a] ($n = 8$)	*P* value
miR-135b	3.71 (3.61–7.67)	6.52 (1.47–9.22)	NS
miR-205	4.95 (3.95–5.79)	5.38 (2.96–7.36)	NS
miR-21	0.24 (0.013–0.45)	0.82 (0.31–1.73)	0.017
miR-30a-3p	0.52 (0.34–0.65)	0.69 (0.52–1.08)	NS
CA125	22.5 (17.6–51.2)	17.5 (7.7–127.4)	NS

Expression levels of miRNAs are described as MoM values [median (minimum — maximum)], and CA 125 levels as U/mL. Significant differences between groups were analyzed by Mann–Whitney *U* test. $P < 0.05$ was considered significant.
NS, not significant.
[a] Includes tumors with more advanced FIGO stage and/or histopathological grade than Stage IA, Grade 1.

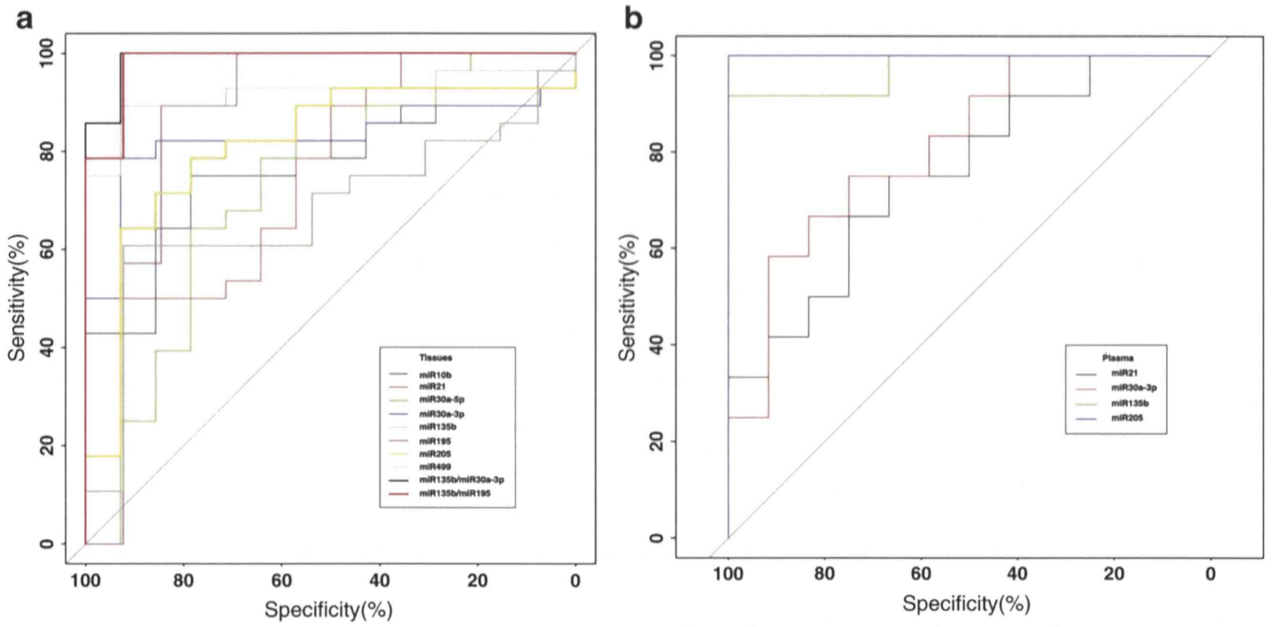

Fig. 1. ROC curve analysis using tissue and plasma miRNA profiles for discriminating EEC samples from NE samples. (A) Tissue miRNA profiles (EEC, $n = 28$; control, $n = 14$); miR-10b, miR-499, miR-195, miR-135b, miR-30a-5p, miR-205, miR-30a-3p and miR-21 yielded AUC of 0.7602 (95% CI: 0.6132–0.9072), 0.7143 (95% CI: 0.5537–0.8749), 0.8736 (95% CI: 0.7145–1.000), 0.9184 (95% CI: 0.8285–1.0), 0.7245 (95% CI: 0.5445–0.9045), 0.8112 (95% CI: 0.666–0.9565), 0.8265 (95% CI: 0.6953–0.9578) and 0.7423 (95% CI: 0.5744–0.9103), respectively. The miR signatures consisting of 2 miRNAs yielded elevated AUC values in comparison to single miRNAs. The miR135b/miR30a-3p yielded an AUC of 0.9898 (95% CI: 0.9677–1.0, $P < 0.038$, Wald test), and miR135b/miR195 yielded AUC of 0.9835 (95% CI: 0.9677–1.0, $P < 0.048$, Wald test). (B) Plasma miRNA profiles (EEC, $n = 12$; control, $n = 12$); miR-135b, miR-205, miR-30a-3p and miR-21 yielded AUC values of 0.9722 (95% CI: 0.913–1.0), 1.0 (95% CI: 1.0–1.0), 0.8125 (95% CI: 0.6381–0.9869), and 0.7569 (95% CI: 0.5611–0.9528), respectively.

advanced tumors was significantly higher than that in tissues of Stages IA and IB tumors. The expression level of miR-205 in EEC of FIGO Grade 3 tumor was significantly higher than that in Grade 1 and 2 tumors. The expression level of has-miR-499 in tissues of FIGO Stage IA and Grade 1 tumors was significantly lower than in tissues of other tumors (FIGO Stage IB or more advanced, and Grade 2 or 3). ROC curve analysis revealed that single regulated EEC-associated miRNAs in tissues could distinguish between EEC and NE tissue samples yielding high AUCs. In addition, 2 miRNA signatures, miR135b/miR195 and miR135b/miR30a-3p, classified EEC tumor tissues with higher accuracy than single miRNAs. These observations suggest that EEC-associated miRNA signatures in tissue could be a diagnostic marker, a supportive marker to estimate the pathological stage and grade of EEC, and potential markers to decide treatment strategies for each EEC case [7].

Finally, as non-invasive markers for EEC, four EEC-associated miRNAs (increased level: miR-135b, miR-205, decreased-level: miR-30a-3p and miR-21) in plasma were identified. Increased levels of EEC-associated miRNAs in plasma also showed higher expression level in EEC tissue, and decreased levels of EEC-associated miRNAs in EEC plasma showed lower expression level in EEC tissue. This suggests that circulating levels of EEC-associated miRNA in plasma reflect the expression status of EEC-associated miRNA in tissue. Torres et al. evaluated miRNA profiles in matched tissue and plasma samples from EEC patients, and showed diagnostic and prognostic significance of plasma miRNA signatures in EEC [7]. Although invasive procedures including biopsies or surgery were performed in the current clinical diagnosis, plasma-based biomarkers may lead to development of a non-invasive test of EEC. To date, miRNA expression pattern is known to be aberrant in cancer, and tumor-cell-derived miRNAs in circulation may be stored in microvesicles that are secreted by various cell types. Additionally, cell-free miRNAs are remarkably stable molecules in plasma [35]. Although the source of plasma EEC-associated miRNAs has not been determined so far, they might derive from exosomes shed from apoptotic or broken cells in EEC and NE [35–37]. In this study, circulating levels of 3 EEC-associated miRNAs (miR-135b, miR-205 and miR-30a-3p) in plasma were significantly decreased after surgery, suggesting that these miRNAs in plasma were mainly from EEC and NE, and may serve as a non-invasive biomarker for diagnosis of EEC, for example, early detection of early-stage EEC or relapse.

As for the clinical significance of plasma EEC-associated miRNAs, circulating levels of EEC-associated miRNAs in plasma were compared in groups distinguished according to FIGO stage and histopathological grade. In comparison of FIGO Stage IA (Grade 1) tumors with others (more advanced FIGO stage and/or histopathological grade), the plasma concentration of miR-21 in cases of FIGO Stage IA (Grade 1) tumors was significantly higher than in more advanced tumors, suggesting that this miRNA may have the potential to detect early-stage EEC. ROC curve analysis revealed that 4 single regulated EEC-associated miRNAs in plasma could distinguish between EEC and NE cases yielding high AUCs (Fig. 1B). Two single miRNAs, miR-135b and miR-205, yielded 0.9722 (95% CI: 0.913–1.0) and 1.0 (95% CI: 1.0–1.0), respectively. CA125 is a current tumor marker for EEC, and can be measured simply and non-invasively, and provide a useful indicator of tumor status. However, the sensitivity and positive predictive value of CA125 is relatively low in detecting EEC [38]. In contrast, EEC-associated miRNAs have different expression profiles in NE and EEC, suggesting that EEC-associated miRNAs in plasma may be used as additional biomarkers for EEC diagnosis.

In conclusion, a set of EEC-associated miRNAs in tissue and plasma of EEC patients was identified by NGS, which could enable in-depth characterization of the global repertoire of miRNAs. EEC-associated miRNA levels in tissue and plasma were associated with pathological characteristics, and could distinguish EEC from NE samples with high accuracy. Although our data are still preliminary because of the small sample size, the measurement of EEC-associated miRNAs in the tissue and plasma may be used as a diagnostic, prognostic, and follow-up test for EEC. Future studies regarding the biological pathway of EEC-associated miRNAs in tissue and plasma may contribute to the elucidation of molecular pathogenesis of EEC, endometrium development, and discovery of novel therapeutic targets of EEC.

Supplementary data to this article can be found online at http://dx.doi.org/10.1016/j.ygyno.2014.01.029.

Conflict of interest

The authors declare no conflict of interest.

Acknowledgments

This work was supported by the Japan Society for the Promotion of Science KAKENHI grant numbers 23592406 and 24791712.

References

[1] Amant F, Moerman P, Neven P, Timmerman D, Van Limbergen E, Vergote I. Endometrial cancer. Lancet 2005;366:491–505.
[2] Matias-Guiu X, Catasus L, Bussaglia E, Lagarda H, Garcia A, Pons C, et al. Molecular pathology of endometrial hyperplasia and carcinoma. Hum Pathol 2001;32:569–77.
[3] Mendell JT. MicroRNAs: critical regulators of development, cellular physiology and malignancy. Cell Cycle 2005;4:1179–84.
[4] Plasterk RH. Micro RNAs in animal development. Cell 2006;124:877–81.
[5] Chung TK, Cheung TH, Huen NY, Wong KW, Lo KW, Yim SF, et al. Dysregulated microRNAs and their predicted targets associated with endometrioid endometrial adenocarcinoma in Hong Kong women. Int J Cancer 2009;124:1358–65.
[6] Ramón LA, Braza-Boïls A, Gilabert J, Chirivella M, España F, Estellés A, et al. MicroRNAs related to angiogenesis are dysregulated in endometrioid endometrial cancer. Hum Reprod 2012;27:3036–45.
[7] Torres A, Torres K, Pesci A, Ceccaroni M, Paszkowski T, Cassandrini P, et al. Diagnostic and prognostic significance of miRNA signatures in tissues and plasma of endometrioid endometrial carcinoma patients. Int J Cancer 2013;132:1633–45.
[8] Jia W, Wu Y, Zhang Q, Gao G, Zhang C, Xiang Y. Identification of four serum microRNAs from a genome-wide serum microRNA expression profile as potential non-invasive biomarkers for endometrioid endometrial cancer. Oncol Lett 2013;6:261–7.
[9] Coppée JY. Do DNA, microarrays have their future behind them? Microbes Infect 2008;10:1067–71.
[10] Yang Q, Lu J, Wang S, Li H, Ge Q, Lu Z. Application of next-generation sequencing technology to profile the circulating microRNAs in the serum of preeclampsia versus normal pregnant women. Clin Chim Acta 2011;412:2167–73.
[11] Pecorelli S. Revised FIGO staging for carcinoma of the vulva, cervix, and endometrium. Int J Gynaecol Obstet 2009;105:103–4 [Erratum in: Int J Gynaecol Obstet 2010;108:176.].
[12] Miura K, Miura S, Yamasaki K, Higashijima A, Kinoshita A, Yoshiura K, et al. Identification of pregnancy-associated microRNAs in maternal plasma. Clin Chem 2010;56:1767–71.
[13] Meyer SU, Pfaffl MW, Ulbrich SE. Normalization strategies for microRNA profiling experiments: a 'normal' way to a hidden layer of complexity? Biotechnol Lett 2010;32:1777–88.
[14] Ng EK, Tsui NB, Lam NY, Chiu RW, Yu SC, Wong SC, et al. Presence of filterable and nonfilterable mRNA in the plasma of cancer patients and healthy individuals. Clin Chem 2002;48:1212–7.
[15] Higashijima A, Miura K, Mishima H, Kinoshita A, Jo O, Abe S, et al. Characterization of placenta-specific microRNAs in fetal growth restriction pregnancy. Prenat Diagn 2013;33:214–22.
[16] Hansen KD, Irizarry RA, Wu Z. Removing technical variability in RNA-seq data using conditional quantile normalization. Biostatistics 2012;13:204–16.
[17] Mortazavi A, Williams BA, McCue K, Schaeffer L, Wold B. Mapping and quantifying mammalian transcriptomes by RNA-Seq. Nat Methods 2008;5:621–8.
[18] Li R, Li Y, Kristiansen K, et al. SOAP: short oligonucleotide alignment program. Bioinformatics 2008;24:713–4.
[19] Robin X, Turck N, Hainard A, Tiberti N, Lisacek F, Sanchez J-C, et al. pROC: an open-source package for R and S+ to analyze and compare ROC curves. BMC Bioinformatics 2011;12:77.
[20] Banno K, Kisu I, Yanokura M, Masuda K, Ueki A, Kobayashi Y, et al. Epigenetics and genetics in endometrial cancer: new carcinogenic mechanisms and relationship with clinical practice. Epigenomics 2012;4:147–62.
[21] Cohn DE, Fabbri M, Valeri N, Alder H, Ivanov I, Liu CG, et al. Comprehensive miRNA profiling of surgically staged endometrial cancer. Am J Obstet Gynecol 2010;202:656 [e1–8].
[22] Chung TK, Lau TS, Cheung TH, Yim SF, Lo KW, Siu NS, et al. Dysregulation of microRNA-204 mediates migration and invasion of endometrial cancer by regulating FOXC1. Int J Cancer 2012;130:1036–45.
[23] Lee JW, Park YA, Choi JJ, Lee YY, Kim CJ, Choi C, et al. The expression of the miRNA-200 family in endometrial endometrioid carcinoma. Gynecol Oncol 2011;12:56–62.
[24] Boren T, Xiong Y, Hakam A, Wenham R, Apte S, Wei Z, et al. MicroRNAs and their target messenger RNAs associated with endometrial carcinogenesis. Gynecol Oncol 2008;110:206–15.
[25] Wu W, Lin Z, Zhuang Z, Liang X. Expression profile of mammalian microRNAs in endometrioid adenocarcinoma. Eur J Cancer Prev 2009;18:50–5.
[26] Torres A, Torres K, Pesci A, Ceccaroni M, Paszkowski T, Cassandrini P, et al. Deregulation of miR-100, miR-99a and miR-199b in tissues and plasma coexists with increased expression of mTOR kinase in endometrioid endometrial carcinoma. BMC Cancer 2012;12:369.
[27] Su N, Qiu H, Chen Y, Yang T, Yan Q, Wan X. miR-205 promotes tumor proliferation and invasion through targeting ESRRG in endometrial carcinoma. Oncol Rep 2013;29:2297–302.
[28] Lee H, Choi HJ, Kang CS, Lee HJ, Lee WS, Park CS. Expression of miRNAs and PTEN in endometrial specimens ranging from histologically normal to hyperplasia and endometrial adenocarcinoma. Mod Pathol 2012;25:1508–15.
[29] Majid S, Saini S, Dar AA, Hirata H, Shahryari V, Tanaka Y, et al. MicroRNA-205 inhibits Src-mediated oncogenic pathways in renal cancer. Cancer Res 2011;71:2611–21.
[30] Nystrom-Lahti M, Parsons R, Sistonen P, Pylkkanen L, Aaltonen LA, Leach FS, et al. Mismatch repair genes on chromosomes 2p and 3p account for a major share of hereditary nonpolyposis colorectal cancer families evaluable by linkage. Am J Hum Genet 1994;55:659–65.
[31] Okuda T, Sekizawa A, Purwosunu Y, Nagatsuka M, Morioka M, Hayashi M, et al. Genetics of endometrial cancers. Obstet Gynecol Int 2010. http://dx.doi.org/10.1155/2010/984013.
[32] Backes FJ, Leon ME, Ivanov I, Suarez A, Frankel WL, Hampel H, et al. Prospective evaluation of DNA mismatch repair protein expression in primary endometrial cancer. Gynecol Oncol 2009;114:486–90.
[33] Tong WG, Ding XZ, Talamonti MS, Bell RH, Adrian TE. LTB4 stimulates growth of human pancreatic cancer cells via MAPK and PI-3 kinase pathways. Biochem Biophys Res Commun 2005;335:949–56.
[34] Zhu F, Park E, Liu B, Xia X, Fischer SM, Hu Y. Critical role of IkappaB kinase alpha in embryonic skin development and skin carcinogenesis. Histol Histopathol 2009;24:265–71.
[35] Kosaka N, Iguchi H, Ochiya T. Circulating microRNA in body fluid: a new potential biomarker for cancer diagnosis and prognosis. Cancer Sci 2010;101:2087–92.
[36] Valadi H, Ekström K, Bossios A, Sjöstrand M, Lee JJ, Lötvall JO. Exosome-mediated transfer of mRNAs and microRNAs is a novel mechanism of genetic exchange between cells. Nat Cell Biol 2007;9:654–9.
[37] Chen X, Liang H, Zhang J, Zen K, Zhang CY. Secreted microRNAs: a new form of intercellular communication. Trends Cell Biol 2012;22:125–32.
[38] Sebastianelli A, Renaud MC, Grégoire J, Roy M, Plante M. Preoperative CA 125 tumour marker in endometrial cancer: correlation with advanced stage disease. J Obstet Gynaecol Can 2010;32:856–60.

Journal of Human Genetics (2014), 1–8

www.nature.com/jhg

ORIGINAL ARTICLE

Identification of two novel mutations in the *NOG* gene associated with congenital stapes ankylosis and symphalangism

Akira Ganaha[1,3], Tadashi Kaname[2,3], Yukinori Akazawa[1,3], Teruyuki Higa[1,3], Ayano Shinjou[1,3], Kenji Naritomi[2,3] and Mikio Suzuki[1,3]

In this study, we describe three unrelated Japanese patients with hearing loss and symphalangism who were diagnosed with proximal symphalangism (SYM1), atypical multiple synostosis syndrome (atypical SYNS1) and stapes ankylosis with broad thumb and toes (SABTT), respectively, based on the clinical features. Surgical findings in the middle ear were similar among the patients. By next-generation and Sanger sequencing analyses, we identified two novel mutations, c.559C>G (p.P178A) and c.682T>A (p.C228S), in the SYM1 and atypical SYNS1 families, respectively. No pathogenic changes were found in the protein-coding regions, exon–intron boundaries or promoter regions of the *NOG*, *GDF5* or *FGF9* genes in the SABTT family. Such negative molecular data suggest there may be further genetic heterogeneity underlying SYNS1, with the involvement of at least one additional gene. Stapedotomy resulted in good hearing in all patients over the long term, indicating no correlation between genotype and surgical outcome. Given the overlap of the clinical features of these syndromes in our patients and the molecular findings, the diagnostic term '*NOG*-related-symphalangism spectrum disorder (*NOG*-SSD)' is advocated and an unidentified gene may be responsible for this disorder.
Journal of Human Genetics advance online publication, 13 November 2014; doi:10.1038/jhg.2014.97

INTRODUCTION

Proximal symphalangism (SYM1) with conductive hearing loss was first described in 1960 by Vesell.[1] In 1999, Gong *et al.*[2] found that mutation in the *NOG* gene was responsible for SYM1. This gene encodes a secreted protein, noggin, a bone morphogenetic protein antagonist essential for normal bone and joint development in humans and mice.[3] *NOG* gene mutations leading to aberrant functions of the noggin protein have been found in some syndromes involving digital anomalies, including SYM1,[1] multiple synostosis syndrome (SYNS1),[4] facioaudiosymphalangism,[5] tarsal–carpal coalition syndrome,[6,7] stapes ankylosis with broad thumb and toes (SABTT)[8] and brachydactyly type B2.[9] Because these syndromes share several overlapping features, it is sometimes difficult to reach an exact diagnosis. Given the overlapping clinical features and shared genetic cause of these syndromes with symphalangism, the collective term *NOG*-related symphalangism spectrum disorder (*NOG*-SSD) was proposed by Potti *et al.*[10] in 2011. Following this proposed terminology, the same mutation in the *NOG* gene was reported in these overlapping syndromes with symphalangism.[2,11] In addition to *NOG* mutations, mutations in *growth differentiation factor-5* (*GDF5*) on chromosome 20q11.2 or in *fibroblast growth factor 9* (*FGF9*) on chromosome 13q12 have been found in patients with SYNS1.[12,13] However, as the GDF5 protein interacts with the NOG protein,[14,15] the diagnostic category of *NOG*-SSD does appear to be promising.

In this study, we present the clinical findings, including surgical results for hearing loss, and the molecular findings of the *NOG*, *GDF5* and *FGF9* genes for three unrelated Japanese patients clinically diagnosed with SYM1, SYNS1 or SABTT. Our results are consistent with the advocated disease category of *NOG*-SSD.

PATIENTS AND METHODS

Three affected patients from unrelated families were investigated. The patients' clinical histories, including hearing loss and symphalangism, were taken and physical examinations, including otoscopy, hearing tests and computed tomography of the temporal bones, were conducted. All patients were examined for the presence of conductive hearing loss, symphalangism, hyperopia, broad thumbs or great toes, syndactyly and fusion of vertebrae. Hearing level was defined as the average of the hearing threshold at 0.5, 1.0, 2.0 and 4.0 kHz determined by pure-tone audiometry. Stapedius reflex tests were performed using standard audiometric procedures and equipment. High-resolution temporal bone computed tomography scans were performed to identify middle or inner ear malformations. All patients underwent radiographic scans to identify possible fusion of the bones in the hands or feet. Stapes surgery was performed in three patients to restore hearing loss.

[1]Department of Otorhinolaryngology-Head and Neck Surgery, University of the Ryukyus, Okinawa, Japan and [2]Department of Medical Genetics, University of the Ryukyus, Okinawa, Japan
[3]These authors contributed equally to this work.
Correspondence: Dr A Ganaha, Department of Otorhinolaryngology-Head and Neck Surgery, University of the Ryukyus, 207 Uehara, Nishihara, Okianwa 903-0215, Japan.
E-mail: ganahaa@med.u-ryukyu.ac.jp
Received 28 August 2014; accepted 12 October 2014

Table 1 Summary of clinical features of three patients

	Hearing level (dB)		*Findings at operation*							
Case	*Right*	*Left*	*Stapes ankylosis*	*Fixed short process*	*Symphalangism*	*Syndactyly*	*Hyperopia*	*Hemicylindrical nose*	*Short distal phalanges*	*Fused cervical vertebrae on roentgenograms*
1	56	56	+	−	+	+	−	−	+	−
2	56	52	+	+	+	−	+	+	−	+
3	66	58	+	−	+	−	+	−	+	−

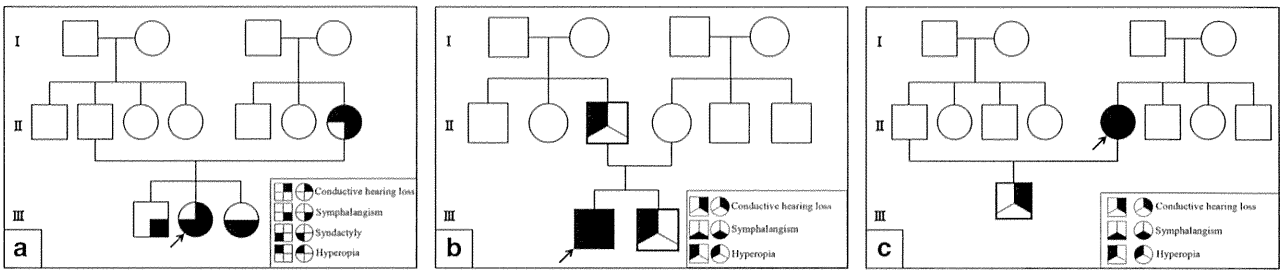

Figure 1 Pedigree of the three reported patients. Pedigrees of (**a**) patient 1 (III-2), (**b**) patient 2 (III-1) and (**c**) patient 3 (II-5).

Before enrollment, all patients provided written informed consent. The research protocol was approved by the Ethical Review Board of the University of the Ryukyus, Japan.

NOG genotyping

Next-generation sequencing. Genomic DNA was extracted from whole blood using a QIAamp DNA Blood Mini Kit (Qiagen, Hilden, Germany). Targeted resequencing of the *NOG* gene, including the promoter region, was performed by next-generation sequencing following long and accurate PCR. The NOG genomic region, spanning 6.5 kb (including a 3.5-kb upstream region), was amplified by long-range PCR with the primer pair 5′-GTCCAAAGGTGTTG GAGTTGATTTCAG-3′ and 5′-AGGCTGTGAGCCTTGTTGATTCCAAG-3′. The amplicon was then purified and fragmented using a Covaris sonicator (Covaris, Woburn, MA, USA). The fragmented DNA was end-repaired and ligated with an adapter for next-generation sequencing. The target DNA was sequenced with a GS Junior System (Roche, Basel, Switzerland).

Sanger sequencing. To confirm the coding sequences and substitutions, the *NOG* gene was Sanger sequenced using three primer pairs (primer sequences are available on request) in six subjects. PCR was performed as follows: initial denaturation at 94 °C for 5 min; 35 cycles of 94 °C for 40 s, 64 °C for 40 s, and 72 °C for 1 min; and a final extension at 72 °C for 5 min. PCRs were run using a programmable thermal cycler (Verti 96-Well Thermal Cycler; Applied Biosystems, Foster City, CA, USA). PCR products were purified using a Wizard SV Gel and PCR Clean-Up System (Promega, Madison, WI, USA) and directly sequenced using an ABI PRISM 3130xl Genetic Analyzer (Applied Biosystems). The sequences obtained were aligned and compared using the BLAST program with known human genome sequences available in the GenBank database.

PCR–restriction fragment length polymorphism analysis of *NOG* mutations in control subjects

We surveyed the substitutions c.559C>G (p.P178A) and c.682T>A (p.C228A) in 200 healthy unrelated Japanese individuals used as controls. The genotypes of the c.559C>G (p.P178A) and c.682T>A (p.C228A) substitutions were detected by digestion of the PCR product with the restriction enzymes *Btg*I and *Hpy*CH4V (both from New England Biolabs, Ipswich, MA, USA), respectively.

In silico analysis of substitutions

The Double Prediction Method[16] was used for predicting the secondary structure of the proteins. To analyze the pathological effect of coding variants on protein function in each substitution, four different prediction programs were used: SIFT (http://sift.jcvi.org),[17] PolyPhen-2 (http://genetics.bwh.harvard.edu/pph2/),[18] PROVEAN (http://provean.jcvi.org)[19] and Mutation Taster.[20]

RESULTS

Case presentation

Table 1 presents a summary of the clinical findings of the three patients (1 man and 2 women; age range, 19–31 years). Patients 1 and 2, whose hearing loss appeared in childhood, wore hearing aids in both ears at the first visit to our hospital. All three patients had no history of ear disease-related hearing loss, such as chronic otitis media or cholesteatoma, and had similar otologic examination results. They had conductive hearing loss in both ears (Figure 3): bone conduction levels in both ears were almost normal and air conduction hearing levels ranged from 70 to 35 dB. They had a type A tympanogram, absence of the stapedius reflex and a normal eardrum under microscopic observation. Computed tomography scan showed no apparent ossicle malformation in either ear in any patient.

Patient 1 (patient III-2 in family 1). A 22-year-old Japanese woman (III-2) was referred to our institution at age 16 years because of hearing loss since early childhood. The family pedigree is illustrated in Figure 1a. Her facial appearance is shown in Figures 2a and b. Her hands showed cutaneous syndactyly between the second and third digits and symphalangism in both distal interphalangeal joints of the fifth fingers (Figures 4a and b). Her feet also showed symphalangism in the third to fifth toes and short first toes of both feet (Figures 5a and b). Symphalangism in both little fingers and short proximal phalanges in both first toes were observed on X-ray examination (Figures 4b and 5b). Ophthalmologic examination displayed no abnormal findings such as hyperopia or strabismus. No facial dysmorphism was observed (Figures 2a and b). She underwent exploratory tympanotomy of the left ear at the age of 16 years that

Figure 2 Facial appearance of the patients. (**a**, **b**) Patient 1 (patient III-2 in family 1). (**c**, **d**) Patient 2 (patient III-1 in family 2). Note the hemicylindrical nose, hypoplastic nasal alae and thin upper vermilion. (**e**, **f**) Patient 3 (patient II-5 in family 3).

revealed ankylosis of the stapes footplate without incus fixation and congenital malformation of the ossicles. Stapedotomy was performed using a Teflon piston. Her postoperative hearing threshold improved to 25 dB in the left ear (Figure 3b) and has been stable for $\geqslant$5 years after the surgery. A diagnosis of SYM1 was made based on the clinical findings.

Patient 2 (patient III-1 in family 2). A 19-year-old Japanese man (III-1) was referred to us because of bilateral hearing loss since early childhood. His family pedigree is illustrated in Figure 1b. His hands showed symphalangism in both proximal interphalangeal joints of the fifth fingers (Figure 4c). Physical and X-ray examination of the feet revealed symphalangism in the fifth toes of both feet (Figures 5c and d). X-ray of the cervical vertebrae revealed fusion of C6–C7 without reduced motion of the neck. He wore glasses for bilateral hyperopia. Dysmorphology examination showed a hemicylindrical nose, hypoplastic nasal alae and thin upper vermilion (Figures 2c and d).

Exploratory tympanotomy in the left ear was performed at age 19 years and revealed ankylosis of the stapes footplate. Only slight immobility without malformation of the incus was detected and was considered acceptable. Stapedotomy was performed using a Teflon piston. His postoperative hearing threshold improved to 25 dB in the operated ear (Figure 3d) and his hearing level has remained stable for more than 2 years after surgery. A diagnosis of SYNS1 was made based on the clinical findings.

Patient 3 (patient II-5 in family 3). A 31-year-old Japanese woman (II-5) was referred to our hospital at age 9 years because of hearing loss since early childhood. The family pedigree is illustrated in Figure 1c. Her facial appearance is shown in Figures 2e and f. Her son has conductive hearing loss without symphalangism or hyperopia. Physical examination of the hands revealed symphalangism in both proximal interphalangeal joints of the fifth fingers (Figure 4e), whereas both feet had symphalangism in the third to fifth toes (Figure 5e). Symphalangism and short intermediate phalanges in both fifth fingers were confirmed by X-ray examination (Figures 4f and 5f). Ophthalmologic examination revealed hyperopia. No facial dysmorphism was observed. Exploratory tympanotomy was performed in the left ear at age 9 years and 5 months later in her right ear. Ankylosis of the stapes footplate without incus fixation and malformation of the ossicles were evident in both ears. Stapedotomy was performed using a Teflon piston in both ears. Her postoperative hearing threshold in the left and right ears improved to 17 and 27 dB, respectively (Figure 3f), and her hearing level has been stable for 22 years after surgery. The diagnosis was SABTT based on the clinical findings.

Genetic analysis

Family 1. Next-generation sequence analysis revealed the presence of a heterozygous substitution in the *NOG* gene, c.559C>G (p.P178A) (Figure 6). The c.559C>G substitution in patient 1 (III-2) was confirmed by direct sequence analysis (Figure 6c). This substitution was not found in 200 controls.

Family 2. Molecular analyses were performed in patient 2 (III-1) and his parents (II-3, II-4). Next-generation sequencing analysis revealed the presence of a heterozygous substitution of the *NOG* gene, c.682T>A (p.C228A) (Figure 6). The c.682T>A substitution was identified in the father (II-3) and son (III-1) but not in the mother (II-4). The heterozygous c.682T>A substitution was confirmed by direct sequence analysis (Figure 6d). This substitution was not found in 200 controls.

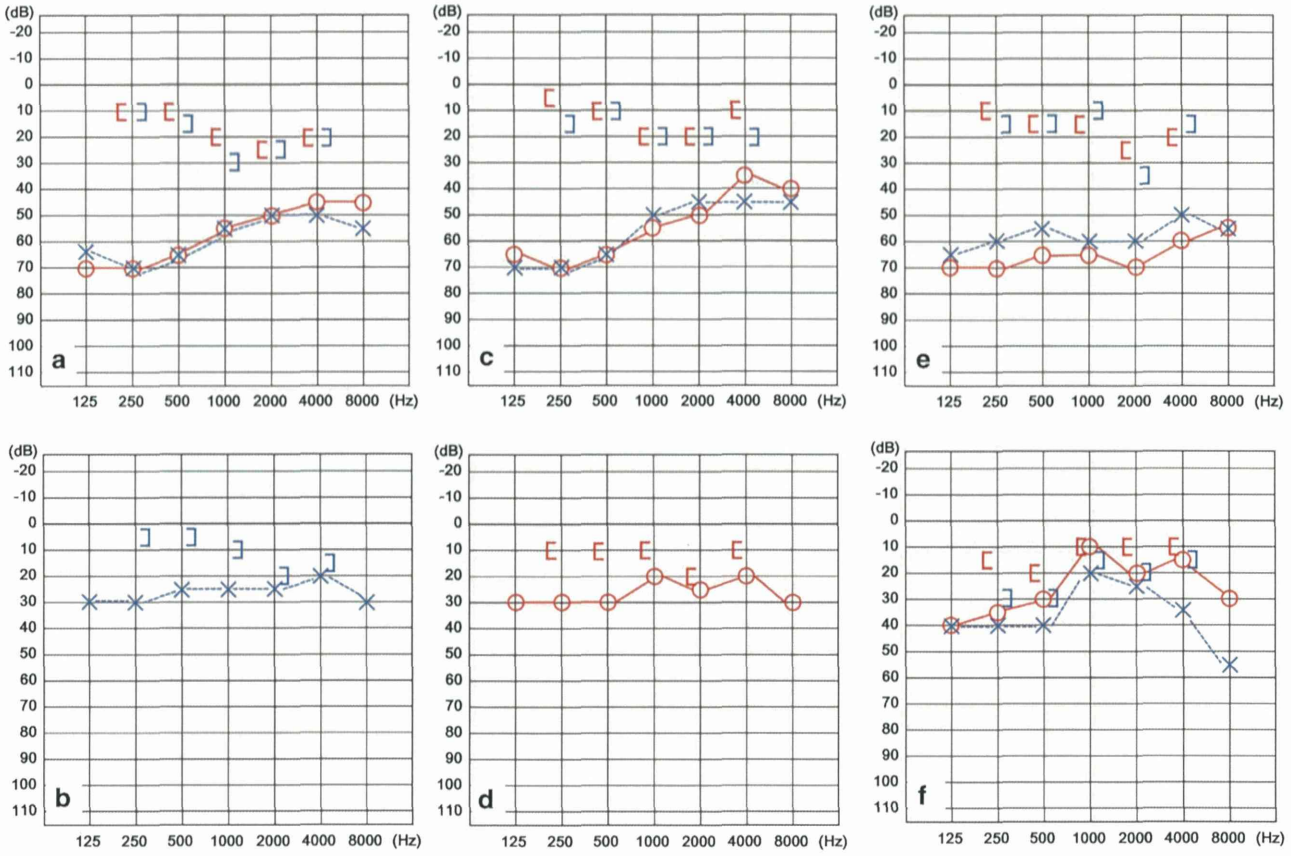

Figure 3 Pure tone audiograms of the patients. Preoperative audiograms of (**a**) patient 1, (**c**) patient 2 and (**e**) patient 3 showing bilateral conductive hearing loss. Postoperative audiograms of (**b**) patient 1, (**d**) patient 2 and (**f**) patient 3 showing improvement in hearing threshold in the operated ear.

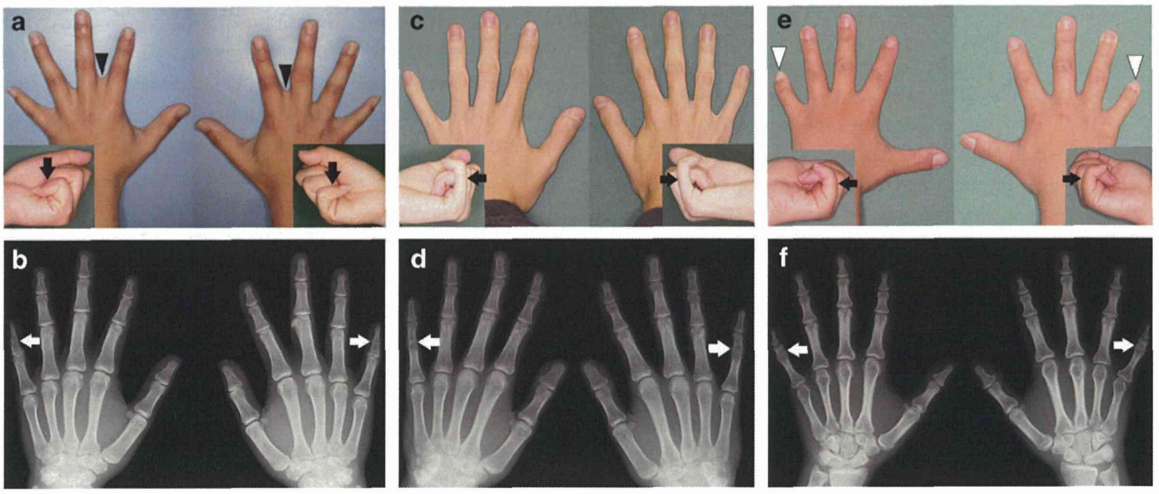

Figure 4 Views and radiographs of the patients' hands. (**a**, **b**) Patient 1, (**c**, **d**) patient 2 and (**e**, **f**) patient 3. (**a**, **c**, **e**) Views of hands and (**b**, **d**, **f**) radiographs of hands. Black arrows indicate symphalangism in (**a**) the distal interphalangeal joint and (**c**, **d**) proximal interphalangeal joint of the fifth fingers. Black arrowheads indicate cutaneous syndactyly. White arrowheads indicate short fifth fingers (brachydactyly).

Family 3. Molecular analyses were performed in patient 3 (II-5) and her son (III-1). Next-generation sequence analysis and direct sequence analysis of the *NOG*, *GDF5* and *FGF9* genes showed no pathogenic mutations in patient 3 (II-4) or her son (III-1) (data not shown).

Analysis of the secondary structure of the NOG protein

We identified two novel mutations, c.559C>G (p.P178A) and c.682T>A (p.C228S), in two of our patients, respectively. The secondary structure of the NOG protein was predicted to be altered

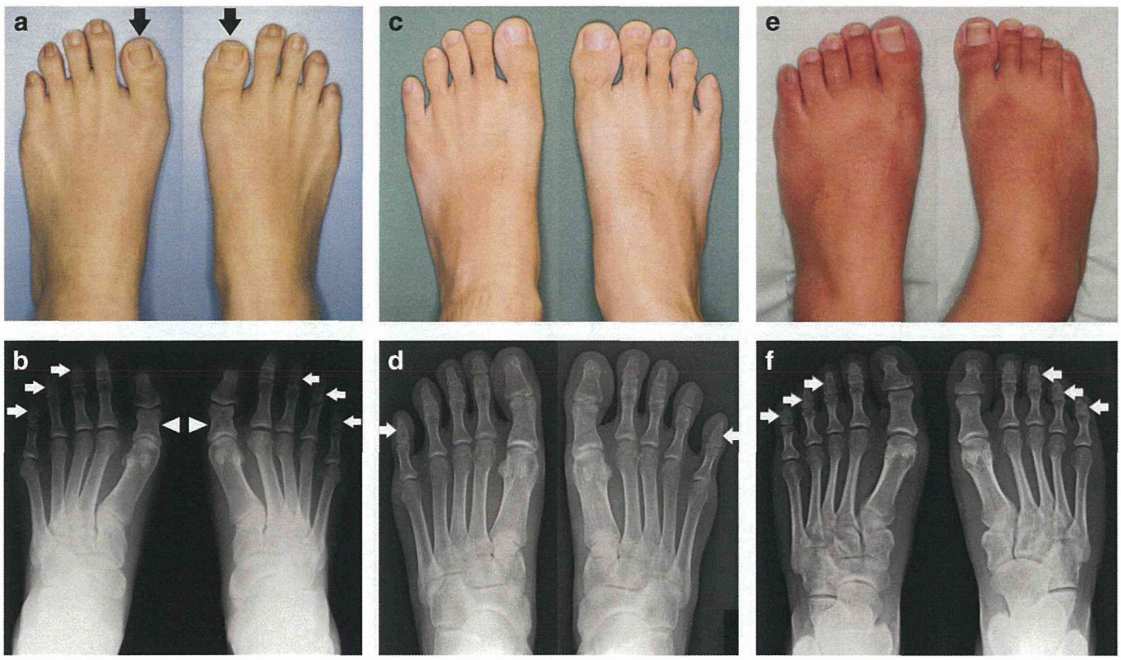

Figure 5 Views and radiographs of the feet of the patients. (**a**, **b**) Patient 1, (**c**, **d**) patient 2 and (**e**, **f**) patient 3. (**a**, **c**, **e**) Views of feet and (**b**, **d**, **f**) radiographs of feet. Black arrows indicate short first toes. White arrows indicate symphalangism. Arrowheads indicate short proximal phalanges (hypoplasia).

from a random coil to an α-helix between A187 and E188 by the mutation of p.P187A (Figures 7a and b), leading to an extended strand between C184 and S185 (Figure 7b). The secondary structure of the mutated NOG protein p.C228S was altered from an extended strand to a random coil between S226 and E227 (Figures 7c and d). These conformational changes may inhibit dimer formation or interaction with other transforming growth factor-β family members, possibly leading to the clinical features constituting the proposed disease category of *NOG*-SSD.

In silico substitution analysis

The four prediction methods used to evaluate the potential impact of amino acid substitutions on the structure and function of the noggin precursor protein revealed that both mutations affected protein function, except for PolyPhen2 for P187A (Table 2).

DISCUSSION

NOG mutations and diseases

We performed molecular investigation of three patients who showed overlapping clinical features of hearing loss and symphalangism. Next-generation and Sanger sequencing analyses revealed two novel mutations, c.559C>G (p.P178A) and c.682T>A (p.C228S), in the SYM1 and atypical SYNS1 families, respectively. These mutations have not been described previously and were not found in 200 controls. The predicted secondary structures of these mutated proteins were different from those of the wild-type protein. The *NOG* region amino acid 178 is located in the dimerization domain.[9] The two novel substitutions of p.P187A and p.C228S affect the dimerization of the NOG protein. SIFT, PROVEAN and Mutation Taster, but not PolyPhen-2, predicted that both substitutions affect protein function. For mutation p.P187A, a different amino acid change at the same position, P187S, has also been reported as a pathological mutation disrupting the dimerization of the NOG protein in a patient with proximal symphalangism.[9] The noggin protein contains seven cysteine residues within the carboxyl terminal region, matching the pattern found in the Kunitz-type protease inhibitor superfamily.[21] The cysteine-rich Kunitz domain can mediate specific interaction with another protein by forming disulfide bonds between cysteine residues. The cysteine knot motif of the C-terminal domain of noggin was disrupted and noggin failed to function when these sites were mutated because of damage to the formation of disulfide bonds in noggin dimerization.[22,23] These data suggest that the two novel substitutions c.559C>G (p.P178A) and c.682T>A (p.C228S) are pathological.

Mutations in the *NOG* gene have been found in several syndromes, including SYM1,[1] SYNS1,[4] facioaudiosymphalangism,[5] tarsal–carpal coalition syndrome,[6,7] SABTT[8] and brachydactyly type B2,[9] leading to the somewhat controversial proposal of the novel category *NOG*-SSD that combines the syndromes.[10] Among our three patients, there is a marked overlap between the SYM1, atypical SYNS1 and SABTT syndromes with respect to the clinical features associated with joint-fusion syndromes (Table 3), supporting their assignment to the same spectrum with phenotypic variation. Further supporting evidence is that the same mutation of p.P35S in the *NOG* gene has been found in both tarsal–carpal coalition syndrome and SYM1.[24] In the present study, variable phenotype expressivity was observed in each family, but our patients had overlapping symptoms with one another. In patient 1, we diagnosed the disorder as SYM1 because typical symptoms of SYM1 were displayed. In patient 2, we diagnosed atypical SYNS1 because the clinical features best matched the diagnostic criteria of SYNS1, although the patient was hyperopic. *NOG* mutations were found in both cases, lending support to the concept of *NOG*-SSD.

NOG-SSD may display locus heterogeneity, given that mutations in other genes such as *GDF5*[12,25] and *FGF9*[13] have been reported in some families with the overlapping syndromes associated with symphalangism. In patient 3, because the diagnosis was typical SABTT, we examined the *NOG* gene, including its promoter region, by next-generation sequencing. However, no mutation was identified in the *NOG* gene or the promoter. We also examined the *GDF5* and *FGF9*

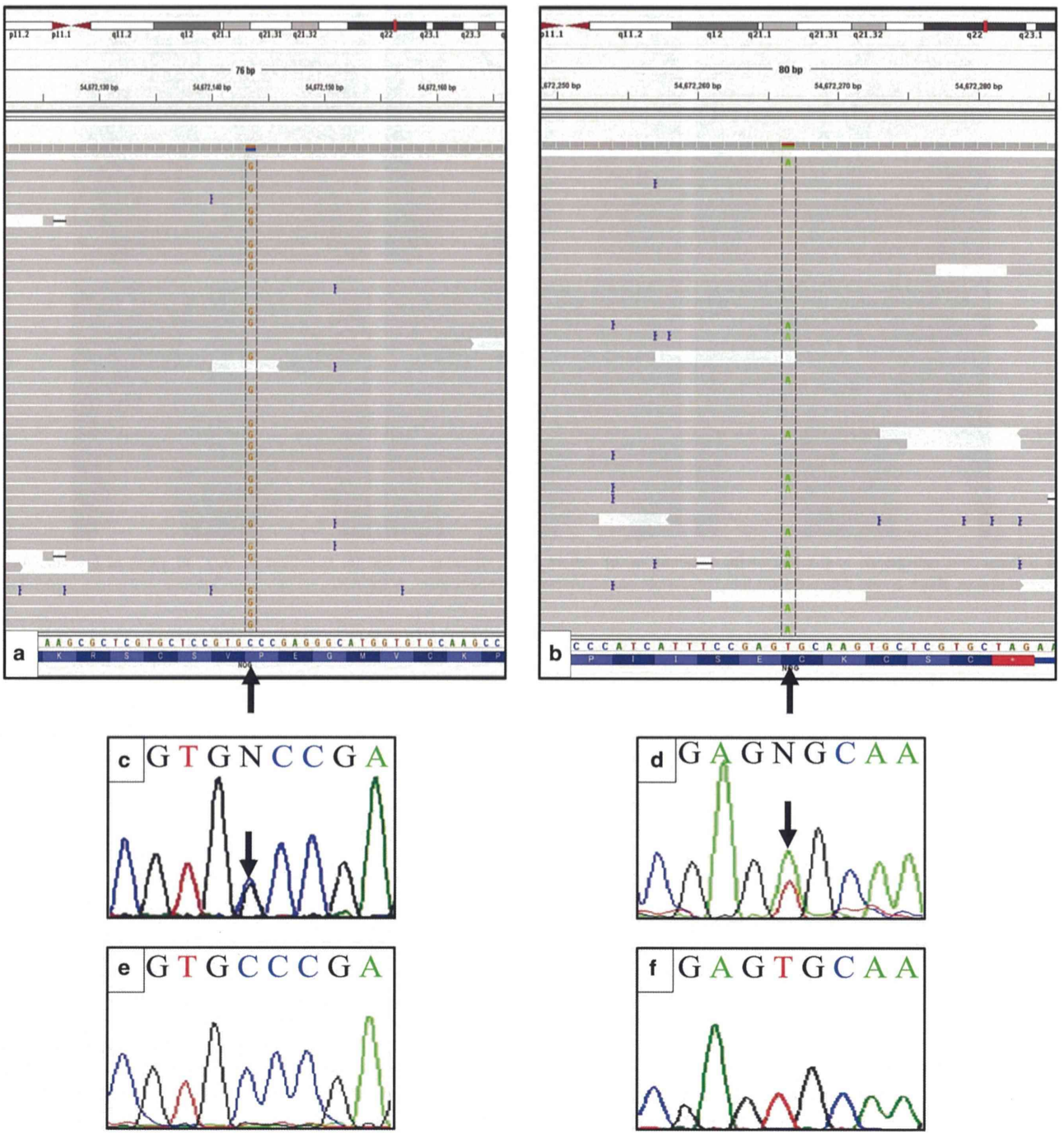

Figure 6 *NOG* gene sequencing profiles for the patients. (**a**, **b**) Integrative genomics viewer images of next-generation sequencing analysis of the *NOG* gene. (**c**–**f**) Sanger sequencing diagram for the (**c**, **d**) patients and (**e**, **f**) wild types. (**a**, **c**) Patient with the c.559C>G (p.P178A) mutation and (**b**, **d**) patient with the c.682T>A (p.C228A) mutation. Arrows indicate the variant nucleotide.

genes in patient 3 by direct and next-generation sequencing, but found no pathological substitutions in the protein-coding regions, exon–intron boundaries or promoter regions of either gene. Such negative molecular data for family 3 indicate that there may be further genetic heterogeneity underlying SYNS1, with the involvement of at least one additional gene. In fact, two studies by Dawson *et al.*[12] and van den Ende *et al.*[26] found no mutations in either *NOG* or *GDF5* in the patient with *NOG*-SSD. Moreover, they did not find any mutations in *NOG*, *BMPR1B*, *GDF5* or *FGF9* in a patient with a clinical phenotype showing features of SYNS1 or facioaudiosymphalangism, suggesting further genetic heterogeneity for these syndromes.

Surgery

In addition to stapes ankylosis, fixation of the short process of the incus in the fossa incudis has been reported in patients with *NOG*-SSD.[8,27–30] In patient with incus fixation, incudal mobilization was required at the time of stapes surgery.[8,27–30] In the present study, fixation of the incus was identified in patient 2, but because the

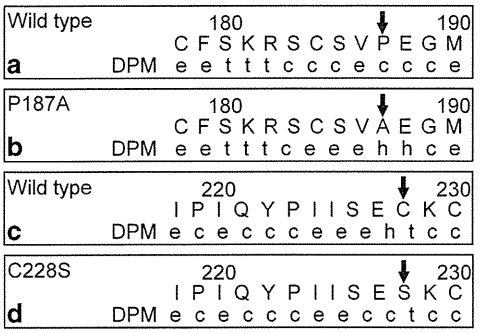

Figure 7 Prediction of the secondary structure of NOG protein. (**a**, **b**) Wild-type P187 and P187A and (**c**, **d**) wild-type C228 and C228S. Arrows indicate targeted amino acids. c, random coil; DPM, double prediction method;[16] e, extended strand; h, α-helix; t, β-turn.

Table 2 Summary of analysis *in silico*

Variant	*PROVEAN*	*SIFT*	*PolyPhen-2*	*Mutation taster*
P187A	Deleterious	Intolerant	Benign	Disease causing
C228S	Deleterious	Intolerant	Probably damaging	Disease causing

Table 3 Phenotypes of symphalangism spectrum disorder and cases of this report

	SYNS1	*SYM1*	*TCC*	*SABTT*	*Case 1*	*Case 2*	*Case 3*
Symphalangism	+	+	+	−	+	+	+
Stapes ankylosis	+	+	−	+	+	+	+
Hyperopia	−	−	−	+	−	+	+
Typical face	+	−	−	+	−	+	−
Fusion of carpal and tarsal bones	+	−	+	−	−	+	−

Abbreviations: SABTT, stapes ankylosis with broad thumb and toes; SYM1, symphalangism; SYNS1, multiple synostosis syndrome; TCC, tarsal–carpal coalition syndrome.

immobility was considered acceptable, incudal mobilization was not performed and the outcome was hearing improvement with mild conductive hearing loss. Disappointing long-term results of stapes surgeries with proximal symphalangism syndrome have been reported.[29,31] The improved hearing threshold after stapes surgery deteriorates during the follow-up period because of a dislocated piston, a process considered to result from bony reclosure of the footplate.[29,31] Thus, partial stapedectomy or stapedectomy should be considered to prevent reclosure of the oval window.[29,31] In the present study, stapedotomy was performed in all patients and all retained good hearing over the long term (between 2 and >20 years). In view of our surgical outcomes, stapes surgery for conductive hearing loss in symphalangism spectrum disorder may be a good therapeutic option. Moreover, as the ossicular condition during surgery was not different among patients, there was no clear relationship between genotype and surgical outcome in our patients.

CONCLUSION

In three patients with overlapping clinical features of hearing loss and symphalangism, we identified two novel mutations, p.P187A and p.C228S, in the SYM1 and atypical SYNS1 families, respectively. The *NOG* gene mutations clearly give rise to a spectrum of clinical findings. The two novel *NOG* mutations identified lend support to the notion of *NOG*-related symphalangism spectrum disorder. We also found no pathogenic changes in the protein-coding regions, exon–intron boundaries or promoter regions of the *NOG*, *GDF5* or *FGF9* genes in the SABTT family, suggesting an unidentified gene may be responsible for this disorder. These two novel mutations and clinical manifestations in patients in this study will contribute to an understanding of *NOG*-SSD.

ACKNOWLEDGEMENTS

This work was supported by the Japan Society for the Promotion of Science (JSPS) KAKENHI Grant-in-Aid for Scientific Research (C) No. 25462649.

1 Vesell, E. S. Symphalangism, strabismus and hearing loss in mother and daughter. *N. Engl. J. Med.* **27**, 839–842 (1960).
2 Gong, Y., Krakow, D., Marcelino, J., Wilkin, D., Chitayat, D., Babul-Hirji, R. *et al.* Heterozygous mutations in the gene encoding noggin affect human joint morphogenesis. *Nat. Genet.* **21**, 302–304 (1999).
3 Zimmerman, L. B., De Jesus-Escobar, J. M. & Harland, R. M. The Spemann organizer signal noggin binds and inactivates bone morphogenetic protein 4. *Cell* **86**, 599–606 (1996).
4 Maroteaux, P., Bouvet, J. P. & Briard, M. L. Multiple synostosis disease. *Nouv. Presse. Med.* **1**, 3041–3047 (1972).
5 Hurvitz, S. A., Goodman, R. M., Hertz, M, Katznelson, M. B. & Sack, Y. The facio-audio-symphalangism syndrome: report of a case and review of the literature. *Clin. Genet.* **28**, 61–68 (1985).
6 Drawbert, J. P., Stevens, D. B., Cadle, R. G. & Hall, B. D. Tarsal and carpal coalition and symphalangism of the Fuhrmann type. Report of a family. *J. Bone Joint Surg. Am* **67**, 884–889 (1985).
7 Gregersen, H. N. & Petersen, G. B. Congenital malformation of the feet with low body height. A new syndrome, caused by an autosomal dominant gene. *Clin. Genet.* **12**, 255–262 (1977).
8 Teunissen, B. & Cremers, W. R. An autosomal dominant inherited syndrome with congenital stapes ankylosis. *Laryngoscope* **100**, 380–384 (1990).
9 Lehmann, K., Seemann, P., Silan, F., Goecke, T. O., Irgang, S., Kjaer, K. W. *et al.* A new subtype of brachydactyly type B caused by point mutations in the bone morphogenetic protein antagonist NOGGIN. *Am. J. Hum. Genet.* **81**, 388–396 (2007).
10 Potti, T. A., Petty, E. M. & Lesperance, M. M. A comprehensive review of reported heritable noggin-associated syndromes and proposed clinical utility of one broadly inclusive diagnostic term: NOG-related-symphalangism spectrum disorder (NOG-SSD). *Hum. Mutat.* **32**, 877–886 (2011).
11 Dixon, M. E., Armstrong, P., Stevens, D. B. & Bamshad, M. Identical mutations in NOG can cause either tarsal/carpal coalition syndrome or proximal symphalangism. *Genet. Med.* **3**, 349–353 (2001).
12 Dawson, K., Seeman, P., Sebald, E., King, L., Edwards, M., Williams, J. 3rd *et al.* GDF5 is a second locus for multiple-synostosis syndrome. *Am. J. Hum. Genet.* **78**, 708–712 (2006).
13 Wu, X. L., Gu, M. M., Huang, L., Liu, X. S., Zhang, H. X., Ding, X. Y. *et al.* Multiple synostoses syndrome is due to a missense mutation in exon 2 of FGF9 gene. *Am. J. Hum .Genet.* **85**, 53–63 (2009).
14 Chang, S. C., Hoang, B., Thomas, J. T., Vukicevic, S., Luyten, F. P., Ryba, N. J. *et al.* Cartilage-derived morphogenetic proteins. New members of the transforming growth factor-beta superfamily predominantly expressed in long bones during human embryonic development. *J. Biol. Chem.* **269**, 28227–28234 (1994).
15 Storm, E. E. & Kingsley, D. M GDF5 coordinates bone and joint formation during digit development. *Dev. Biol.* **209**, 11–27 (1999).
16 Deleage, G. & Roux, B. An algorithm for protein secondary structure prediction based on class prediction. *Protein Eng.* **1**, 284–294 (1987).
17 Ng, P. C. & Henikoff, S. Predicting deleterious amino acid substitutions. *Genome Res.* **11**, 863–874 (2001).
18 Adzhubei, I. A., Schmidt, S., Peshkin, L., Ramensky, V. E., Gerasimova, A., Bork, P. *et al.* A method and server for predicting damaging missense mutations. *Nat. Methods* **7**, 248–249 (2010).
19 Choi, Y., Sims, G. E., Murphy, S., Miller, J. R. & Chan, A. P. Predicting the functional effect of amino acid substitutions and indels. *PLoS ONE* **7**, e46688 (2012).
20 Schwarz, J. M., Rödelsperger, C., Schuelke, M. & Seelow, D. Mutation Taster evaluates disease-causing potential of sequence alterations. *Nat. Methods* **7**, 575–576 (2010).
21 McDonald, N. Q. & Kwong, P. D. Does noggin head a new class of Kunitz domain? *Trends Biochem. Sci.* **18**, 208–209 (1993).
22 Liu, W., Ren, C., Shi, J., Feng, X., He, Z., Xu, L. *et al.* Characterization of the functionally related sites in the neural inducing gene noggin. *Biochem. Biophys. Res. Commun.* **270**, 293–297 (2000).

23 Rudnik-Schöneborn, S., Takahashi, T., Busse, S., Schmidt, T., Senderek, J., Eggermann, T. *et al.* Facioaudiosymphalangism syndrome and growth acceleration associated with a heterozygous NOG mutation. *Am. J. Med. Genet. A* **152A**, 1540–1544 (2010).
24 Hirshoren, N., Gross, M., Banin, E., Sosna, J., Bargal, R. & Raas-Rothschild, A. P35S mutation in the NOG gene associated with Teunissen-Cremers syndrome and features of multiple NOG joint-fusion syndromes. *Eur. J. Med. Genet.* **51**, 351–357 (2008).
25 Wang, X., Xiao, F., Yang, Q., Liang, B., Tang, Z., Jiang, L. *et al.* A novel mutation in GDF5 causes autosomal dominant symphalangism in two Chinese families. *Am. J. Med. Genet. A* **140A**, 1846–1853 (2006).
26 van den Ende, J. J., Borra, V. & Van Hul, W. Negative mutation screening of the NOG, BMPR1B, GDF5, and FGF9 genes indicates further genetic heterogeneity of the facioaudiosymphalangism syndrome. *Clin. Dysmorphol.* **22**, 1–6 (2013).
27 Thomeer, H. G., Admiraal, R. J., Hoefsloot, L., Kunst, H. P. & Cremers, C. W. Proximal symphalangism, hyperopia, conductive hearing impairment, and the NOG gene: 2 new mutations. *Otol. Neurotol.* **32**, 632–638 (2011).
28 Weekamp, H. H., Kremer, H., Hoefsloot, L. H., Kuijpers-Jagtman, A. M., Cruysberg, J. R. & Cremers, C. W. Teunissen-Cremers syndrome: a clinical, surgical, and genetic report. *Otol. Neurotol.* **26**, 38–51 (2005).
29 Ensink, R. J., Sleeckx, J. P. & Cremers, C. W. Proximal symphalangism and congenital conductive hearing loss: otologic aspects. *Am. J. Otol.* **20**, 344–349 (1999).
30 Cremers, C., Theunissen, E. & Kuijpers, W. Proximal symphalangia and stapes ankylosis. *Arch. Otolaryngol.* **111**, 765–767 (1985).
31 Brown, D. J., Kim, T. B., Petty, E. M., Downs, C. A., Martin, D. M., Strouse, P. J. *et al.* Characterization of a stapes ankylosis family with a NOG mutation. *Otol. Neurotol.* **24**, 210–215 (2003).

Ecotoxicology
DOI 10.1007/s10646-014-1307-6

Establishment of a primary hepatocyte culture from the small Indian mongoose (*Herpestes auropunctatus*) and distribution of mercury in liver tissue

Sawako Horai · Kumiko Yanagi · Tadashi Kaname · Masatatsu Yamamoto · Izumi Watanabe · Go Ogura · Shintaro Abe · Shinsuke Tanabe · Tatsuhiko Furukawa

Accepted: 6 August 2014

Abstract The present study established a primary hepatocyte culture for the small Indian mongoose (*Herpestes auropunctatus*). To determine the suitable medium for growing the primary hepatic cells of this species, we compared the condition of cells cultured in three media that are frequently used for mammalian cell culture: Dulbecco's Modified Eagle's Medium, RPMI-1640, and William's E. Of these, William's E medium was best suited for culturing the hepatic cells of this species. Using periodic acid-Schiff staining and ultrastructural observations, we demonstrated the cells collected from mongoose livers were hepatocytes. To evaluate the distribution of mercury (Hg) in the liver tissue, we carried out autometallography staining. Most of the Hg compounds were found in the central region of hepatic lobules. Smooth endoplasmic reticulum, which plays a role inxenobiotic metabolism, lipid/cholesterol metabolism, and the digestion and detoxification of lipophilic substances is grown in this area. This suggested that Hg colocalized with smooth endoplasmic reticulum. The results of the present study could be useful to identify the detoxification systems of wildlife with high Hg content in the body, and to evaluate the susceptibility of wildlife to Hg toxicity.

Keywords Small Indian mongoose · Primary hepatocyte culture · Hepatic lobule · AMG staining · Mercury distribution

Introduction

Mercury (Hg), one of the most toxic elements, is commonly found in the global environment, and is present at very high concentrations in marine mammals (Wagemann et al. 1998; Cardellichio et al. 2000; Fant et al. 2001; Woshner et al. 2001; Cardellicchio et al. 2002; Chen et al.

Electronic supplementary material The online version of this article (doi:10.1007/s10646-014-1307-6) contains supplementary material, which is available to authorized users.

S. Horai (✉)
Department of Regional Environment, Tottori University, 4-101 Koyamacho-Minami, Tottori 680-8551, Japan
e-mail: horais@rs.tottori-u.ac.jp

K. Yanagi · T. Kaname
Department of Medical Genetics, University of the Ryukyus School of Medicine, Okinawa, Japan

M. Yamamoto · T. Furukawa
Department of Molecular Oncology, Graduate School of Medical and Dental Sciences, Kagoshima University, Kagoshima, Japan

I. Watanabe
Department of Environmental Conservation, Tokyo University of Agriculture and Technology, Tokyo, Japan

G. Ogura
Department of Subtropical Agro-Environmental Sciences, University of the Ryukyus, Okinawa, Japan

S. Abe
Naha Nature Conversation Office, Ministry of the Environment, Tokyo, Japan

S. Tanabe
Center for Marine Environmental Studies, Ehime University, Ehime, Japan

Published online: 21 August 2014

2002; Monteiro-Neto et al. 2003; Ikemoto et al. 2004a, b; Lemes et al. 2011). Marine mammals that have high Hg contents in their livers may have a prominent detoxification system in this organ. The ratio of organic Hg(O-Hg) to total Hg(T-Hg) tends to be higher in individuals with low T-Hg content than in those with high T-Hg contents in the liver. This shows that demethylation of methyl Hg is promoted in the body, particularly in the liver (Caurant et al. 1996; Meador et al. 1999; Cardellichio et al. 2000; Cardellicchio et al. 2002). In addition, a positive correlation between Se and T-Hg was found in marine mammals with high T-Hg in the liver (Caurant et al. 1996; Wagemann et al. 1998; Meador et al. 1999; Fant et al. 2001; Woshner et al. 2001; Cardellicchio et al. 2002; Endo et al. 2002; Decataldo et al. 2004). It is generally accepted that the Hg toxicity is reduced by being bonded with selenium (Wagemann et al. 1998; Cardellichio et al. 2000; Endo et al. 2002; Arai et al. 2004). Mercuric selenide (HgSe) and/or HgS which are considered as inert nontoxic compounds have been found in higher trophic marine mammals, such as striped dolphin (Ng et al. 2001), northern fur seal and black-footed albatross (Arai et al. 2004). Although the first report on marine mammals with high Hg in their bodies was made by Koeman et al. (1973), the detail Hg detoxification system is not yet identified in these apparently Hg-tolerant animals.

It has been found that the amount of Hg in the atmosphere increased as much as threefold since the beginning of the industrial revolution (Lindberg et al. 2007). The primary sources of Hg are natural, anthropogenic, and re-emitted sources (Environmental Protection Agency (US) 1997). Globally, approximately 2,000–2,200 tons of Hg is released annually into the atmosphere from anthropogenic sources, representing two-thirds of the total release (Seigneur et al. 2004). Recently, increasing temporal trends of Hg in wildlife and ecosystems have been reported (Rigét et al. 2011; Sonne et al. 2012; Blévin et al. 2013). Rigét et al. (2011) reported that most of the Hg level increasing data sets in Arctic biota was marine species, especially marine mammals. Methylmercury is the only species of Hg to get concentrated in each successive level in the food chain, reaching levels in predatory fish that are about a million times higher than in seawater (Mason et al. 2012; Krabbenhoft and Sunderland 2013). Fish are the main methylmercury exposure source for most wildlife species and human (Krabbenhoft and Sunderland 2013). In human, effects of chronic low-level methylmercury exposure showed long-term neurocognitive deficits in children, impaired cardiovascular health and immune system in adults (Karagas et al. 2012). In vitro assay of methylmercury on peripheral blood mononuclear cells (PBMCs) of harbor seal revealed that the number of lymphocytes, viability, metabolic activity, DNA and RNA synthesis decreased, suggesting deleterious effects of methylmercury concentrations naturally encountered in free-ranging seals (Das et al. 2008). Therefore, Hg level of exposure to wildlife, particularly marine mammals, has increased, and, accordingly, understanding Hg toxicity and detoxification mechanisms in wildlife is an urgent issue.

In vivo and in vitro assays are generally available for determination of the toxicity and detoxification mechanisms of chemicals including Hg. There are few reports on in vitro assays of Hg using wildlife, harbor seal PBMCs (Das et al. 2008; Dufresne et al. 2010), grey seal PBMCs (Dufresne et al. 2010) and beluga whale lymphocytes (Frouin et al. 2012), whereas in vivo assays using marine mammals have never been reported. These techniques seem to be difficult to use for marine mammals in view of their body weights and lengths, and protective measures of conservation and so on.

The Javan mongoose (*Herpestes javanicus*) has been exterminated as it is an alien species in Japan. In our previous study, we observed that the Javan mongoose (*Herpestes javanicus*) had high Hg levels in the liver similar to those reported for marine mammals. A positive correlation and 1:1 molar ratio between Se and T-Hg was also found in the liver of Javan mongoose (Horai et al. 2006). In addition, O-Hg/T-Hg ratio degradation with increasing of T-Hg concentration was observed in the liver of this species similar to those of marine mammals (Horai et al. 2006). These results raise the possibility that the liver of Javan mongoose has Hg metabolism and/or detoxification system similar to those of marine mammals. We considered Javan mongoose as an animal model for wildlife that has high Hg content in the liver as in marine mammals.

Primary hepatocytes are supposed to synthesize and secrete serum proteins, synthesize and decompose glycogen, and metabolize xenobiotics in a similar way as in the whole liver in vivo (Miyazaki and Namba 1992), substantiating the possibility that in vitro assays of Hg using primary hepatocytes of wildlife, which has high Hg content in the liver, may disclose in vivo Hg detoxification and metabolism in those wildlife. There is no information on Hg-in vitro assays using primary hepatocytes from wildlife, whereas some studies using those from experimental animals, such as rat (Hasgekar et al. 2006) and mouse (Toyama et al. 2011) are available. Different media are available for primary hepatocyte culture studies such as Earle's modified Eagle's medium (MEM) (Hasgekar et al. 2006) or William's E medium (Sashi et al. 2013) for rat hepatocytes, William's E medium (Toyama et al. 2011) or Dulbecco's Modified Eagle's Medium (DMEM) (Chang and Hughes-Fulford 2014) for mouse hepatocytes. First, to establish primary mongoose hepatocyte culture, therefore, we should determine the most suitable medium for it.

The purpose of the present study is to isolate and establish primary hepatocyte culture from mongoose liver using screening of appropriate medium, PAS staining and ultrastructural observation, and to understand the Hg distribution in these hepatocytes using AMG staining.

Though mongoose inhabits Japan had been recognized as Javan mongoose (*Herpestes javanicus*), its genome analysis identified this species in Japan as the small Indian mongoose (*Herpestes auropunctatus*) by Watari et al. (2011). Therefore, we described this species in this study not Javan mongoose (*Herpestes javanicus*) but the small Indian mongoose (*Herpestes auropunctatus*).

Materials and methods

Sample collection

Three adult specimens of the small Indian mongoose, *Herpestes auropunctatus* (2 males and 1 female) were used for the establishment of a primary hepatocyte culture. Male and female hepatocyte cultures were used in the analysis, without further differentiation between sexes. In the present study, we evaluated only adult mongooses. One adult female mongoose was used for PAS staining and AMG staining. One adult female mongoose was used for electron microscopy. They were collected from Okinawa, Japan in 2007 and 2008 as a part of a program to control harmful wildlife.

With regard to the way of animal sacrifice, there are three major methods to sacrifice experimental animals, guillotine, anesthetization and CO_2 gas. We think guillotine is the best method for sacrifice as it will not effect various metabolisms in the body. However, mongoose is a wild animal, and so it is difficult to fix it under the guillotine without anesthetization even though anesthetization and CO_2 gas could change some metabolic processes in the body. Moreover, anesthetization is much less painful than CO_2 gas. In the present study, we have used the same experimental conditions for both mongooses and rats. Therefore we presume that the results can be compared.

All of the animal handling protocols were approved by the Animal Ethics Committee of Ehime University (approval number: 35N32).

Primary hepatocyte culture

Primary hepatocytes were cultured using the method of Sato and Miyazaki Sato and Miyazaki (1984) with slight modification. In brief, mongooses were anesthetized using pentobarbital. The dose was 35 mg kg^{-1} body weight which was referred a previous work by Ishibashi et al. (2009). After the anesthesia took effect, the body was rinsed with 70 % ethanol, and was fixed to a dissecting table. The skin and abdominal muscles were cut with sterilized dissecting scissors. The first 100 mL perfusate was warmed to 37 °C and flowed into the portal vein at a rate of 10 mL min^{-1}. After the perfusate had permeated the entire liver, the abdominal inferior vena cava was cut in order to remove the blood and perfusate from the body. After the first 100 mL perfusate, a second perfusate was administered. The dose and flow speed was the same as for the first perfusate. After the second perfusate, the liver became less cohesive. The liver was removed, placed in a 50 mL conical tube, and fragmented in the second perfusate. The fragmented sample was centrifuged ($50\times g$, 2 min, 4 °C), and then the supernatant was discarded. The precipitated sample was rinsed with 10 mL Hank's solution (Life Technologies, Pleasanton, CA) and centrifuged ($50\times g$, 2 min, 4 °C) again. Rinsing and centrifugation was repeated three times. To remove red blood cells from the sample, 10 mL cold red blood cell lysis buffer was added to the sample. After allowing the sample to settle for 5 min, the sample was centrifuged ($50\times g$, 5 min, RT). This step was repeated three times, resulting in a sample of hepatic cells that was collected from mongoose liver. A total of 5×10^8, 1×10^9 and 1×10^9 cells were collected from the three mongoose livers, respectively. The hepatic cells were cultured in one of three media: DMEM (Life Technologies), RPMI-1640 (DS Pharma Biomedical, Osaka, Japan), or William's E (Sigma-Aldrich, St. Louis, MO) supplemented with 10 % heat inactivated fetal bovine serum, 1 μM insulin, 0.1 mg mL^{-1} kanamycin, 0.5 μg mL^{-1} amphotericin B in collagen-coated dishes. The cell culture has repeated more than twenty times, and the collected cells were used for assays when the cell number was over 10^8 order.

Periodic acid-Schiff (PAS) staining

Glycogen storage of the isolated cells was evaluated by Periodic acid-Schiff (PAS) staining (Wislocki 1950) on day 3 after hepatocyte isolation. The isolated cells were cultured on a poly-L-lysine (PLL)-coated glass slide and fixed with 20 % Mildform® for 20 min. Then the cells were oxidized in 1 % periodic acid solution for 10 min, washed and treated with Schiff's reagent for 15 min, with subsequent color development in sulfite solution for 9 min. To compare isolated hepatic cells with liver tissue, a liver section was also stained with periodic acid Schiff reagents as control.

Autometallography (AMG) staining

AMG staining is a histochemical method to metal and metal compounds such as ZnS, ZnSe, Au, BiS, BiSe, AgS, AgSe, HgS and HgSe (Danscher and Stoltenberg 2006). While the AMG staining is broad for such all materials, the

staining specificity can be narrowed by pretreatments of removing non-target materials. ZnSe, Au, BiS, AgS and AgSe can be removed by exposure of 0.5–2 % KCN for 10 s to 30 min. ZnS can be removed by treatment of 0.1 N HCl. Since BiSe and Hg compounds are resistant to such KCN and HCl pretreatment, the combination with the pretreatments and AMG development detects those materials as particles in the light microscope (Stoltenberg and Danscher 2000).

We performed according to the method described by Danscher and Stoltenberg (2006) with slight modification. In brief, the liver perfused with PBS was collected, fixed with 20 % Mildform, embedded in paraffin and sectioned at 6 μM. The sections were dipped in 1 % Farmer solution (1 % Sodium thiosulphate–0.1 % Potassium ferricyanide) for 10 s and in 0.5 % gelatin solution before mounting onto gelatin-coated slides. Deparaffinized and rehydrated sections were exposed to HCl or KCN to selectively remove certain metal and metal compounds such as ZnS, ZnSe, Au, BiS, AgS and AgSe, but not BiSe, HgS and HgSe (Stoltenberg and Danscher 2000). The Hg compounds were developed as silver nano clusters in silver acetate solution containing hydroquinone (AMG development) (Danscher and Stoltenberg 2006). The liver from an adult female rat housed in a specific pathogen free facility condition was used as control.

Electron microscopy

The mongoose liver and the cultured cells on glass slides were fixed with 2 % glutaraldehyde 2 % paraformaldehyde in 0.1 M PBS. Ultrastructure of them was observed using H-7600 (HITACHI, Japan) operating at 100 kV (performed in Hanaichi Ultra Structure Research Institute (Aichi, Japan)).

Hg analysis

Each part of the liver tissues after the second perfusate treatment were dried at 80 °C for 16 h, and then uniformly homogenized to a fine powder. The samples were dried on petri dishes covered with Teflon sheets. After that the dried samples were homogenized using porcelain mortar and pestle. Approximately 0.2 g of each sample was digested in a microwave system (Ethos D, Milestone S.r.I., Sorisole, BG, Italy) with nitric acid (Nacalaitesque, SP grade for hazardous metal analysis). The Hg level was determined using a Hg analyzer (Model HG-300; Hiranuma, Tsukuba, Japan) with a cold vapor technique. The accuracy of the method was assessed using the standard reference material DOLT-4 (National Research Council Canada) in triplicate. Recoveries of Hg ranged from 100–103 %.

Results and discussion

Selection of a primary hepatocyte culture medium for mongoose

The cells isolated from mongoose livers were maintained in RPMI-1640, DMEM or William's E medium for 72 h. Morphology of the cells was observed every 24 h by phase-contrast microscope. The cells were attached on collagen-coated dishes after 24 h. The cells had polygonal shape with one or two round nuclei that were morphologically compatible with hepatocyte. There was no recognizable difference among the cell-morphologies cultured in three media in 24 h (Fig. S1, Supporting Information). From 24 to 48 h of the culture, considerable cells were detached from the dishes in RPMI-1640 and DMEM. The attached cells decreased clearly in volume of the cytoplasm in DMEM in 72 h. A typical morphologically different cells were recognized in RPMI-1640 in 48 h (Fig. S2, Supporting Information). These morphological changes became more obvious in 72 h (Fig. 1). Morphological examination with phase-contrast microscope, therefore, indicated that William's E was the most suitable medium among the three media used for dose experiments, intake and excretion tests of Hg up to 72 h using the isolated cells.

The compositional unit of liver tissue is the hepatic lobule (Wakui and Kaneda 2001). There is a central vein in the central region of each hepatic lobule, and hepatic cords are radially arranged around the central vein (Wakui and Kaneda 2001). Hepatic parenchyma is composed of hepatocytes and four types of sinusoid cells, including endothelial cells, hepatic stellate cells, Kupffer cells and pit cells (Wakui and Kaneda 2001). Wakui and Kaneda (2001) reported that the hepatocytes accounted for 78 % of cells, whereas sinusoid cells accounted for 6 % of cells in human liver. To confirm that the collected cells were mainly hepatocytes, not fibroblasts which exist in extra-parenchyma cellular space, we carried out PAS staining. Glycogen is stored in hepatocytes (Wakui and Kaneda 2001); therefore, the cells are stained by PAS staining. Collected primary cells were stained similar for a liver tissue section (Fig. 2).

Next, cell structures between the collected primary cells and hepatocytes in the liver were compared using electron microscope (Fig. 3). With regard to characteristics of hepatocyte, one or two bigger nucleus, development of rough-surfaced endoplasmic reticulum and Golgi apparatus, enriched mitochondria, and lysosome near bile canaliculus are generally observed (Wakui and Kaneda 2001). Ultrastructure observations in the present study revealed that a cell had one or two round nuclei, and nucleoli were shown clearly in a nucleus of both the primary cells and the hepatocytes in the liver. Ultrastructure observations further

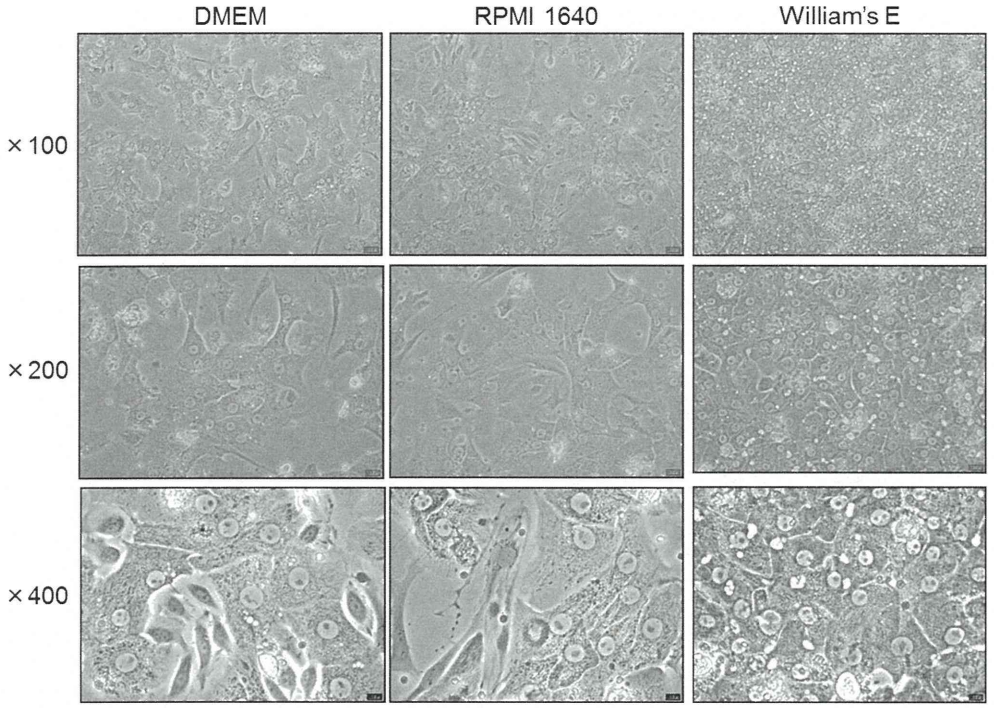

Fig. 1 Comparison of primary hepatic cells isolated from the small Indian mongoose after 72 h culture in three different media

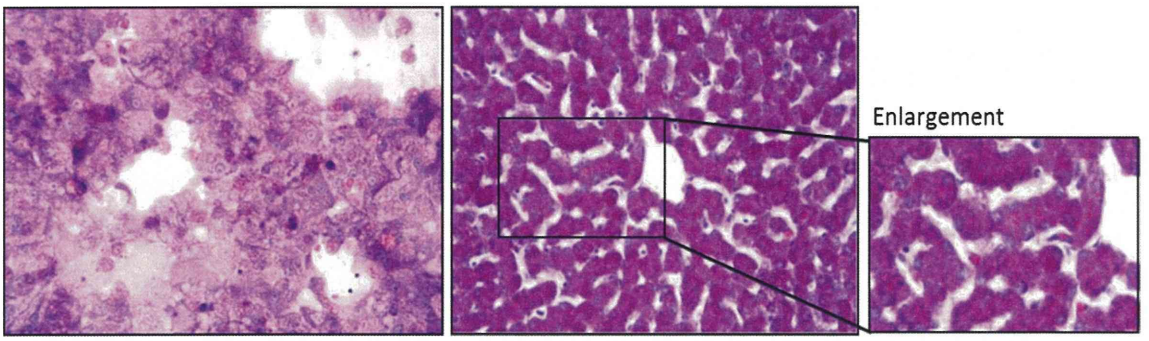

Fig. 2 PAS staining of primary hepatic cells (*left*) and the liver (*right*) in the small Indian mongoose. The magnification is ×400 each

indicated that enriched mitochondria and endoplasmic reticulum, lipid droplet, waste pigment existed in both the primary cells and the hepatocytes in tissue. Microvilli which enable to intake proteins and other plasma constituents from sinusoid to hepatocytes were also observed in the primary cells and the hepatocytes in the liver (Fig. 3, arrow heads). In the isolated primary cells, two lysosomes were found clearly (Fig. 3, upper right), and rough-surfaced endoplasmic reticulum was clearly observed in the hepatocyte of the liver (Fig. 3, lower right). On the other hand, these mongoose individuals were possibly under starvation, because few glycogen granules, which are rich in normal hepatocyte, and some waste pigments were observed. These ultrastructural characteristics of the primary cells were similar to the hepatocytes in the liver. Therefore, these results demonstrated that the primary hepatic cells isolated from the mongoose liver were hepatocytes, and that a primary hepatocyte culture in mongoose had been established.

Hg distribution in hepatic tissue

To demonstrate what metal particles exist in the mongoose liver, we performed AMG staining after the pretreatments. KCN resistant particles were observed in central legion of the hepatic lobules even after pretreatment with 2 % KCN for 30 min (Fig. 4, upper). Particles were also detected after pretreatment with 0.1 N HCl (data not shown). In contrast, these particles were not detected in the rat liver (Fig. 4, lower). Bismuth–Se and Hg(–S, Se) cannot be